AERIS: Eco-Driving Application Development and Testing

FINAL REPORT

FHWA-JPO-12-045

June 2012

U.S. Department of Transportation

Research and Innovative Technology Administration

Virginia Polytechnic Institute and State University
Charles E. Via, Jr. Department of Civil and Environmental Engineering
3500 Transportation Research Plaza
Blacksburg, VA 24061

and

Virginia Tech Transportation Institute
Center for Sustainable Mobility,
3500 Transportation Research Plaza
Blacksburg, VA 24061

TECHNICAL REPORT DOCUMENTATION PAGE

1. Report No. FHWA-JPO-12-045	2. Government Accession No.	3. Recipient's Catalog No.
4. Title and Subtitle AERIS: Eco-Driving Application Development and Testing		5. Report Date June 2012 6. Performing Organization Code:
7. Author(s) Hesham A. Rakha, Kyoungho Ahn, and Sangjun Park		8. Performing Organization Report No.
9. Performing Organization Name and Address Virginia Polytechnic Institute and State University 3500 Transportation Research Plaza Blacksburg, VA 24061 and Virginia Tech Transportation Institute Center for Sustainable Mobility 3500 Transportation Research Plaza Blacksburg, VA 24061		10. Work Unit No. 11. Contract or Grant No.
12. Sponsoring Agency Name and Address United States Department of Transportation, Research and Innovative Technology Administration 1200 New Jersey Ave, S.E. Washington, DC 20590		13. Type of Report and Period Covered Final 14. Sponsoring Agency Code
15. Supplementary Notes		
16. Abstract This exploratory study investigates the potential of developing an Eco-Driving application that utilizes an eco-cruise control (ECC) system within state-of-the-art car-following models. The research focuses on integrating predictive cruise control and optimal vehicle acceleration and deceleration controllers within car-following models to minimize vehicle fuel consumption levels. This system makes use of topographic information, spacing to lead vehicle, and a desired (or target) vehicle speed and distance headway as input variables.		
17. Key Words AERIS, Vehicle emissions reduction strategies, eco-driving, eco-cruise control system, vehicle fuel consumption modeling, vehicle powertrain modeling	18. Distribution Statement No restrictions. Document available from: National Technical Information Services, Springfield, Virginia 22161	

19. Security Class if. (of this report) Unclassified	20. Security Class if. (of this page) Unclassified	21. No. of Pages 47	22. Price

Form DOT F 1700.7 (8-72) Reproduction of completed page authorized

Table of Contents

1 Abstract

This exploratory study investigates the potential of developing an Eco-Driving application that utilizes an eco-cruise control (ECC) system within state-of-the-art car-following models. Roadway grade is one of the major variables that affect vehicle fuel consumption levels. On upgrade sections, vehicles utilize additional power to overcome the grade resistance, thus consuming more fuel than under normal conditions. Typical cruise control systems can consume excessive fuel by trying to maintain a preset speed when the vehicle encounters hilly terrain. If a vehicle tries to maintain a preset speed on a steep uphill section, the vehicle could consume significant amounts of fuel and produce significant greenhouse gas emissions. Thus energy-efficient operations on hilly roads could produce significant savings in fuel consumption usage. The proposed research focuses on integrating predictive cruise control and optimal vehicle acceleration and deceleration controllers within car-following models to minimize vehicle fuel consumption levels. This developed system makes use of topographic information, spacing to lead vehicle, and a desired (or target) vehicle speed and distance headway as input variables. The results of the exploratory study show that the proposed system can significantly reduce vehicle fuel consumption levels while maintaining reasonable vehicle spacing distances. One of the test vehicles, a Toyota Camry, saved 27 percent in fuel consumption with an average spacing of 48 m along a study section of Interstate 81. The study also demonstrates that vehicle operations at lower power demands enhance vehicle fuel economy (up to 49 percent) but not as significantly as the use of the ECC system (which improves fuel economy by up to 82 percent). The study also demonstrates that ECC-equipped vehicles benefit following vehicles. In particular, following vehicles significantly decrease their fuel consumption level just by following the lead ECC-equipped vehicle.

2 Introduction

The transportation sector is responsible for nearly two-thirds of the total gasoline consumption in the United States, so the potential benefits of such a system are significant. Even small fuel consumption reductions could significantly reduce greenhouse gas (GHG) emission levels and increase fuel cost savings.

This study demonstrates the feasibility of an Eco-Driving application that would improve vehicle fuel economy and reduce GHG emissions. In support of a proposed full study, this exploratory study focused its efforts on developing an eco-cruise control system (ECC) within state-of-the-art car-following models. The feasibility of the proposed system was evaluated using a computer simulation to compare the proposed system to data from real driving. Because CO_2 emissions are directly associated with fuel use, the results presented in this study are also applicable to vehicle tailpipe CO_2 emissions.

There are several variables that affect vehicle fuel consumption levels. Roadway grade is one of the major variables that affect vehicle fuel consumption levels. On upgrade

sections, vehicles utilize additional power to overcome the grade resistance, thus consuming more fuel than under normal conditions. Typical cruise control systems can consume excessive fuel by trying to maintain a preset speed when the vehicle encounters hilly terrain. If a vehicle tries to maintain a preset speed on a steep uphill section, this segment could consume significant amounts of fuel and produce significant greenhouse gas emissions. Thus energy-efficient operations on hilly roads could produce significant savings in fuel consumption usage.

A recent study investigated the potential for developing ECC systems that will allow vehicles to travel within a desired speed range instead of driving at a single desired speed regardless of the fuel economy implications.(1) The system utilizes the gravitational force to allow vehicles to travel at higher speeds (within the upper bound of the desired speed) while traveling downhill and travel at lower speeds (within the lower bound of the desired speed) while traveling upgrade sections. The study used vehicle powertrain and fuel consumption models that it developed to evaluate such an application. The ECC-equipped vehicle drove a 26-mi section of Interstate 81 between Roanoke and Blacksburg, Virginia. The results are very promising and indicate potential savings of up to 10 percent in fuel consumption depending on the input speed range.

Another study also developed an eco-predictive cruise control system that utilizes topographical data to develop proactive vehicle control strategies that minimize the vehicle's fuel consumption.[2] The system incorporates ECC system logic through the use of a moving-horizon dynamic programming algorithm with powertrain and fuel consumption models to determine the optimal throttle level, speed, and gear shift points with the objective of minimizing the vehicle's fuel consumption. However, to more easily interpret the system's performance, the eco-predictive cruise control system assumed no interference by other vehicles.

The study focuses on developing predictive ECC algorithms within state-of-the-art car-following models that integrate predictive cruise control that can optimize vehicle acceleration and deceleration controllers with car-following models, as illustrated in Figure 1. The predictive system solves an optimization problem to minimize vehicle fuel consumption levels using road topographical data where the route of a vehicle is known.

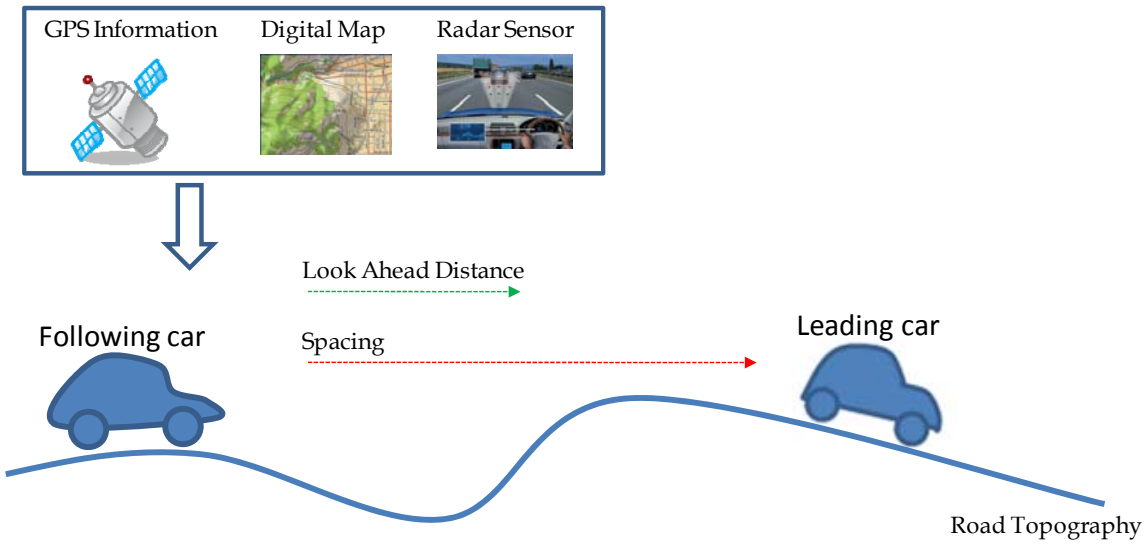

Figure 1. Overview of an eco-driving application

The objective of this exploratory study is to investigate possible fuel savings associated with the proposed Eco-Driving application, which utilizes an ECC system within state-of-the-art car-following models. The system makes use of topographic information, the spacing between the subject and lead vehicle, and a desired (or target) vehicle speed and distance headway as input variables.

3 Previous Studies

3.1 Environmental Effects of Eco-Driving

The popular Web site Ecodriving.org defines eco-driving as "a way of driving that reduces fuel consumption, greenhouse gas emissions and accident rates" and "about driving in a style suited to modern engine technology: smart, smooth and safe driving techniques that lead to average fuel savings of 5-10%".[3] Eco-driving refers to driving techniques that maximize fuel economy and correspondingly reduce GHG. Eco-driving is considered the most cost-effective method of improving road safety and the quality of the environment as well as saving fuel costs. A recent report estimated that teaching consumers to eco-drive can improve actual fuel efficiency by an average of 17 percent.[4]

It is important to understand the factors that affect vehicle fuel consumption and driving behavior. El-Shawarby, et al. investigated the impact of vehicle cruise speed and acceleration levels on vehicle fuel consumption rates and emission rates using field data gathered under real-world driving conditions.[5] The study demonstrated that as the aggressiveness of acceleration maneuvers increased, the fuel consumption and emission rates significantly increased. Several research efforts have quantified the impact of aggressive driving on fuel consumption and emission levels .[6-12] One study from Sierra Research found that aggressive driving is responsible for 15 times higher CO emissions

and 14 times higher HC emissions on the same trip.[13] A recent study demonstrated that 1 percent of a highway trip is responsible for 16, 19, 4, and 3 percent of the total HC, CO, NO_X, and CO_2 emissions, respectively, and 4 percent of the fuel consumption.[14] Furthermore, the study demonstrated that 25 percent of total CO_2 emissions and 28 percent of fuel consumption levels are caused by 10 percent of the most aggressive driving maneuvers of typical trips. The study demonstrated that small portions of a trip produce high engine-load conditions and that reducing these events can significantly improve air quality and fuel economy levels. The results suggest that educating drivers can significantly improve air quality and energy consumption.

3.1.1 Eco-Driving within a Network

Kobayashi, Tsubota, and Kawashima investigated the impacts of eco-driving within a traffic network. They performed field measurements of a vehicle's speed and acceleration versus normal and eco-driving styles and utilized a microscopic simulation model for evaluations. The study found that an eco-driving control system is effective in a traffic network and does not impede traffic flow that would promote traffic congestion.[15] Similarly, researchers from the University of California examined potential environmental benefits of green driving strategies with Next Generation Simulation (NGSIM) data on I-80 near Berkeley, California. The study examined GHG emissions before and after applying green driving strategies. The study found that green driving strategies are most effective for traffic flows with average speeds around 50 km/h and that potential savings can be from 20 to 60 percent for different pollutants.[16]

3.1.2 Eco-Driving Education and Tools

Empirical studies have shown positive relationships among driving behavior, vehicle fuel consumption, and GHG emissions. Several researchers have focused on improved driving patterns and evaluating their impact on vehicle fuel consumption and GHG emissions. An experimental study investigated the impacts of eco-driving, or "technical driving," which optimizes engine speed and torque, and demonstrated substantial savings in fuel consumption and GHG emissions.[17] A Greek eco-driving pilot program found that smart, smooth, and safe driving techniques can lead to potential fuel savings of 10 to 15 percent.[18] The study investigated the effects of modifying urban bus drivers' behavior through training courses on economical and ecological driving. Larsson and Ericsson (2009) quantified the impact of an acceleration advisor on vehicle fuel consumption and emission levels. They developed an acceleration advisor tool that produces a resistance in the accelerator pedal when the driver aggressively accelerates. The study found that aggressive acceleration behaviors were significantly reduced when the acceleration advisor provided advice to drivers, which indicated that the drivers had complied with the advisor.[19] According to a recent pilot study (2010) performed by the University of California at Riverside, participants who utilized an on-board eco-driving device improved fuel economy by approximately 6 percent on local city trips and 1 percent on highway trips.[20]

3.1.3 Advanced Eco-Driving Tools

In addition to strategies that limit maximum acceleration, several in-vehicle technologies, such as various eco-driving systems and driver feedback systems, have been developed to help drivers further reduce fuel consumption and emission levels.[21-23] Van Der Voort developed a prototype fuel-efficiency-supporting tool that advises drivers on essential behavioral adjustments.[24] The system back-calculates the minimum fuel consumption for previous driving schedules and examines if the actual fuel consumption deviates from the minimum fuel consumption. Then the system suggests to the driver ways to change driving patterns. Based on driving simulation tests, this eco-driving system was able to reduce overall fuel consumption by 16 percent. While the typical eco-driving system provides the driver static advice on smooth vehicle acceleration levels that reduce excessive vehicle speeds, Barth and Boriboonsomsin studied the possibility of a dynamic eco-driving system.[25] The proposed system provides real-time, dynamic advice to drivers by using a traffic management system that monitors traffic conditions in the vehicle's vicinity and then communicates advice in real time back to the driver. Based on simulation and real-world vehicle experimentation, the dynamic eco-driving system was found to reduce vehicle fuel consumption and GHG emissions by 10 to 20 percent without drastically affecting overall travel time.

Researchers from Toyota developed a system to promote eco-driving and safe driving.[26] A unit called Behavioral Context Addressable Loggers in the Shell (BCALs) wirelessly communicates driving data to a server and eight (five for eco-driving and three for safe driving) evaluation indicators are provided to a system manager and drivers to review the driving behavior. The study concluded that the users effectively accept the system, which functionally changes driver behavior to be greener and safer. Nissan launched "Vehicle Carte Service," an off-board eco-driving support service, on the company's Web site in 2007.[27] The eco-driving service offers driving data information, including fuel consumption ranking and eco-driving tips. Members compare their eco-driving score with other members in a game environment. The study found that the fuel economy of participants were improved by 18 percent on average.

While most of the studies found that an eco-driving tool can help reduce fuel consumption and GHG emissions, one study found that an eco-driving system may negatively affect drivers. Lee found that the increased cognitive utilization of an eco-driving system may produce negative effects on gas mileage. The study found that users were constantly thinking, deciding, and calculating to improve vehicle fuel efficiency. The study recommended that the eco-driving system should unconsciously adjust their driving behavior. The study also found that driver age and driving experience are important factors when evaluating an eco-drive system.[28]

3.2 Vehicle Optimal Controls

As described earlier, driving style can have a significant impact on vehicle fuel consumption levels, but it is not clear how drivers should control the car to achieve the best possible fuel economy. Several research efforts investigated vehicle optimal speed controls to minimize fuel consumption and GHG emission levels. One of the earliest

research efforts to compute optimal vehicle control was performed by Schwarzkopf and Leipnik (1977). The study developed a highway driving algorithm that can be used to accelerate smoothly from a stop and assists in driving in hilly terrain.[29] Pontriagin's maximum principle method was used to solve the mathematically optimal performance. Hooker also estimated optimal speed control strategies for fuel economy in several typical driving situations: optimal acceleration to cruise speed, optimal driving between stop signs, and optimal driving over hills. The author claimed that optimal speeds are generally higher for larger cars and higher on downgrades than on upgrades, and that the relative fuel penalty for exceeding the speed limit is no worse for small cars than large cars.[30-31]

While the previous research efforts focused on light-duty vehicles, the DaimlerChrysler Research Centre developed a predictive cruise control (PCC) system that can reduce fuel consumption of heavy-duty trucks.[32] The PCC system utilizes a three-dimensional road map and GPS location information to obtain the vehicle's current location and information on the next 4 km ahead of the truck. To reduce fuel consumption, the system allows vehicles to travel within a desired speed range instead of driving at a single desired speed. The simulation results showed that test trucks were able to reduce fuel consumption by 2.61 to 5.16 percent on a 25-km section of I-5 around Portland, Oregon.

Various studies use a control theory approach, but Chang and Morlok assumed that fuel consumption is approximately proportional to the propulsive work and enabled the derivation of the optimal speed profile with respect to minimizing propulsive work.[33] The method is comparatively more direct than other studies. The study also generalized the solution for application to cars and rail.

Hellstrom and his colleagues developed a PCC system for heavy trucks.[34-37] While the system utilizes a similar concept as that used in the DaimlerChrysler Research Center study, Hellstrom utilized advanced control methods, including a vehicle powertrain module and a fuel consumption model. The PCC system repeatedly solved an optimization problem by means of a tailored dynamic programming algorithm. The study assumed that roadway topographical data were available and that the vehicle routing was known.

Saboohi and Farzaneh improved the vehicle optimal control by considering the gear ratio.[38,39] They introduced an optimal model of vehicle fuel consumption that was developed on the basis of microeconomic theories. The model used simulations to estimate the optimal fuel consumption of a vehicle in a given real case and was able to save 37 percent of potential energy consumption. Similarly, Saerens studied the minimization of the fuel consumption of a gasoline engine through dynamic optimization using an engine model and a drive-train model.[40] In this study, the throttle valve angle was utilized as a control input and Bock's direct multiple shooting method was used to determine optimal trajectories for engine speed and throttle valve angle. The method is a numerical technique to solve boundary value problems and is considered as a significant improvement in distribution of nonlinearity and numerical stability.

While most of the optimal control methods estimate vehicle speed profiles minimizing fuel consumption, Kamil et al. developed an eco-driving system using predictive control, which considers future road-traffic situations.[41-43] The researchers developed on-board eco-driving system control that operated in a varying road-traffic environment. The study utilized a combination of Continuation and Generalized Minimum Residual Methods to optimize the sequence of vehicle control actions required in the prediction horizon while maintaining safe driving. The authors evaluated the proposed system through simulations in the AIMSUN NG microscopic simulation program.

3.3 Adaptive Cruise Control (ACC) Models

Adaptive cruise control (ACC) systems automatically adjust a vehicle's preset speed to maintain a preset safe following distance using forward-looking radar.[44] Several researchers are investigating the environmental performance of these automatic control systems.

Ioannou and Stefanovic (2005) pointed out that the smoothing feature of ACC vehicles could improve the fuel efficiency of mixed traffic flow. While the smooth response of the ACC vehicles has a beneficial effect on the environment, the ACC system may disturb the driver when it reacts to high-acceleration maneuvers, lane cut-ins, and lane exits. The authors claimed that the environmental benefits would vary with the levels of disturbance, the position of the ACC vehicle in the string of manually driven vehicles, and the percentage of ACC vehicles on the road.[45] Similarly, Zhang and Ioannou developed a nonlinear, filter-based controller for heavy trucks that restricted acceleration levels to fulfill fuel saving requirements.[46] The filtering effect of trucks was shown to have beneficial effects on fuel economy and pollution. However, it created large inter-vehicle gaps that invited cut-ins from neighboring lanes, creating additional disturbances.

The reduction of fuel consumption usually decreases the acceleration performance and lowers the proper car following capability. This leads to two problems: 1) when the preceding car accelerates, larger inter-vehicular distances occur due to the deficient acceleration performance, resulting in frequent vehicle cut-ins from adjacent lanes, and 2) when the preceding vehicle decelerates, inter-vehicular distance shortens quickly and rear-end collisions are more likely.

To ensure safety and good tracking capability, Corona et al. applied a hybrid model predictive control (MPC) approach to vehicular-following control.[47] Similarly, Kohut et al. designed a predictive control strategy that optimizes the engine torque to trade off reduced fuel consumption for trip time while keeping the vehicle within a specified speed envelope.[48]

Bageshwar et al. presented an MPC-based headway control algorithm with acceleration limitations incorporated explicitly to meet the requirements of ride comfort and safe driving.[49] Li et al. and Luo et al. introduced multiple objectives to achieve the desired driver response, minimal fuel consumption, and minimization of car-following error.[50,51] They employed MPC theory to develop an ACC algorithm that simultaneously satisfied

such control objectives as effective tracking capability, high fuel economy, driver desired response, and collision avoidance.

The literature review has revealed a significant amount of research in predictive eco-cruise control systems; however, no attempt has been made to integrate such systems within car-following controllers.

4 The Building Blocks of the Eco-Driving System

4.1 Fuel Consumption Models

Vehicle fuel consumption levels are typically derived from a relationship between instantaneous fuel consumption rates and instantaneous measurements of various explanatory variables, including vehicle power, force (or tractive effort), acceleration, speed, and roadway grade. Many fuel consumption models incorporate different explanatory variables to satisfy their specific objectives. One variable that stands out is vehicle power or vehicle specific power, which is the power exerted by a vehicle per unit mass. Vehicle power can be computed as the product of the total force exerted by the vehicle and the vehicle velocity. The total force includes both the net force and the force that is required to overcome the aerodynamic, rolling, and grade resistance forces. Assuming that the vehicle fuel consumption rate is proportional to the vehicle power, the fuel consumption can be estimated by computing the forces acting on the vehicle.

Post et al. developed a fuel consumption model based on the instantaneous power demand.(52) The model was built from chassis dynamometer experiments of 177 in-use vehicles. The instantaneous vehicle fuel consumption rate was then computed using the vehicle power as a single independent variable as

$$F(t) = \begin{cases} a_1 + b_1 P(t) & P(t) \geq 0 \\ a_1 & P(t) < 0 \end{cases}$$

Figure 2. Instantaneous vehicle fuel rate

where $F(t)$ is the instantaneous fuel consumption rate in liters per second (l/s), α_1 is the vehicle idling fuel consumption rate (l/s), β_1 is the vehicle fuel consumption rate per unit of power (l/s/kW), and $P(t)$ is the instantaneous total power in kilowatts (kW). Vehicle parameters α_1 and β_1 were found to vary with time as the vehicle's condition and state of tune altered. The on-road instantaneous total power ($P(t)$) was computed as the sum of drag, inertial, and gradient power. Consequently, the instantaneous total power demand is a function of the vehicle speed, speed squared, speed cubed, and the product of speed and acceleration.

The Australian Road Research Board (ARRB) fuel consumption model was developed using the Post model.(53,54) The major difference between the ARRB and Post models is a detailed examination of the β parameter. According to the ARRB study, an average β value does not provide accurate results because the β value varies as a function of the vehicle's instantaneous speed and acceleration level. To improve the accuracy of the Post

model in predicting fuel consumption rates during constant-speed driving as well as acceleration, the authors adopted two efficiency parameters, β_a and β_b, and allowed for an engine/internal drag component to be part of the total drag power. The equation in **Figure 3** demonstrates the general form of the ARRB model, where $P_c(t)$ is the total drag power exerted while traveling at a constant speed (kW), $P_a(t)$ is the total engine/inertia drag power (kW), α_2 is the vehicle's idling fuel consumption rate (l/s), and β_a and β_b are vehicle-specific power parameters (l/s/kW).

$$F(t) = a_2 + b_a P_a(t) + b_b P_c(t)$$

Figure 3. General form of the ARRB model

The Comprehensive Modal Emissions Model (CMEM) is another model that estimates the instantaneous fuel consumption rate based on power, engine friction, engine speed, and vehicle engine size (or displacement).[55,56] The model predicts second-by-second tailpipe emissions and fuel consumption rates for a wide range of vehicle and technology categories. Vehicle operational variables (such as speed, acceleration, and road grade) and model-calibrated parameters (engine friction factor) are utilized as input to estimate vehicle tractive power. The model uses the stoichiometric air/fuel ratio and the in-use air/fuel ratio of the moment to estimate the vehicle fuel consumption rate.

Currently, researchers frequently use vehicle specific power (VSP) to estimate instantaneous vehicle fuel consumption and emission rates.[57,58] VSP is a measure of the engine load and is defined as the power exerted per unit mass to overcome the road grade, rolling, and aerodynamic resistance forces, in addition to the inertial acceleration, and is a function of the vehicle speed, speed cubed, and interaction of speed and acceleration as

$$VSP(t) = f(v, v^3, va)$$

Figure 4. Vehicle specific power

Another fuel consumption model that makes use of topographic and gear shifting information was developed by researchers from Linkőpings University.[37,59-61] The model estimates real-time fuel consumption rates using control signals, such as a pedal, brake, and gear signal, with engine speed, as summarized in the equation shown in **Figure 5**, where N is the number of engine cylinders, n_r is the number of crankshaft revolutions per stroke, $\omega_e(t)$ is the engine speed at any instant t, $f_p(t)$ is the pedal control input [0,1] at any instant t, G is the gear signal, and F_{idle} is the idling fuel consumption rate.

$$F(t) = \begin{cases} \frac{N}{60000 n_r} \times w_e(t) f_p(t) \left(a_d w_e(t)^2 + b_d w_e(t) + c_d \right) & \text{for } G \neq 0 \\ F_{idle} & \text{for } G = 0 \end{cases}$$

Figure 5. Linkőpings University fuel consumption model

While the majority of fuel consumption models were developed as power-demand models, the VT-Micro model was developed as a statistical model from experimentation with numerous polynomial combinations of speed and acceleration levels to construct a dual-regime model as described in the equation in **Figure 6**, where $L_{i,j}$ are model regression coefficients at speed exponent i and acceleration exponent j, $M_{i,j}$ are model regression coefficients at speed exponent i and acceleration exponent j, v is the instantaneous vehicle speed in kilometers per hour (km/h), and a is the instantaneous vehicle acceleration (km/h/s). The model was developed utilizing a number of data sources, including data collected at the Oak Ridge National Laboratory (ORNL) (9 vehicles) and the Environmental Protection Agency (EPA, 101 vehicles). These data included fuel consumption and emission rate measurements (CO, HC, and NO_x) as a function of the vehicle's instantaneous speed and acceleration levels. The VT-Micro fuel consumption and emission rates were found to be highly accurate compared to the ORNL data, with coefficients of determination ranging from 0.92 to 0.99. A more detailed description of the model derivation is provided in the literature.(62)

$$F(t) = \begin{cases} \exp\left(\sum_{i=1}^{3}\sum_{j=1}^{3} L_{i,j} v^i a^j\right) & \text{for } a \geq 0 \\ \exp\left(\sum_{i=1}^{3}\sum_{j=1}^{3} M_{i,j} v^i a^j\right) & \text{for } a < 0 \end{cases}$$

Figure 6. VT-Micro model

Typical power-based fuel consumption models result in a bang-bang type of control system. In other words, the optimal fuel consumption level is achieved by either accelerating at full throttle or decelerating at maximum braking. Such a type of model results in a sub-optimal control system. Bang-bang control occurs when the partial derivative of the fuel consumption rate with respect to the engine torque is not a function of torque, or when

$$\frac{\partial F(t)}{\partial T} = f(T)$$

Figure 7. Bang-bang control

Furthermore, all models described require the collection of field data to calibrate the model parameters. This exercise is time consuming and requires that some form of vehicle instrumentation be implemented to gather field data and develop the models.

The research team for the proposed system has developed two new power-based microscopic fuel consumption models, Virginia Tech Comprehensive Power-based Fuel consumption Models (VT-CPFM-1 and VT-CPFM-2). The models can estimate instantaneous fuel consumption and CO_2 emission levels as required for the proposed eco-driving system. The detailed description of the fuel consumption models is found in Rakha et al.(63)

The developed fuel consumption models utilize instantaneous power as an input variable and can be calibrated using publicly available fuel economy data (city and highway fuel

consumption rates). The models are demonstrated to estimate vehicle fuel consumption rates consistent with in-field measurements (coefficient of determination above 0.75). Finally, the research team developed a procedure for estimating CO_2 emissions that are highly correlated with field measurements (greater than 95 percent). The new fuel consumption models overcome two main deficiencies of current state-of-the-art models: the inability to produce a control system that (1) does not result in bang-bang control and (2) is easily calibrated using publicly available data without the need to gather detailed engine and fuel consumption data.

The two models (VT-CPFM-1 and VT-CPFM-2) are formulated as in **Figure 8** and **Figure 9**:

$$FC(t) = \begin{cases} a_0 + a_1 P(t) + a_2 P(t)^2 & \text{" } P(t) \text{ ³ } 0 \\ a_0 & \text{" } P(t) < 0 \end{cases}$$

Figure 8. VT-CPFM-1

$$FC(t) = \begin{cases} b_0 w(t) + b_1 P(t) + b_2 P(t)^2 & \text{" } P(t) > 0 \\ b_0 w_{idle} & \text{" } P(t) \text{ £ } 0 \end{cases}$$

Figure 9. VT-CPFM-2

where α_0, α_1, α_2 and β_0, β_1, and β_2 are model constants that require calibration, *P(t)* is the instantaneous total power, $\omega(t)$ is the engine speed at any instant *t*, and ω_{idle} is the idling engine speed.

The major difference of two models is the usage of engine speed data. The first model (VT-CPFM-1) does not require any engine data while the second model (VT-CPFM-2) requires additional engine speed data as illustrated in Figure 9. This exploratory study used only VT-CPFM-1 model in order to reduce the complexity of the simulation procedure. It should be noted that the power exerted by a vehicle is a function of the vehicle speed and acceleration, which can be measured directly using a GPS.

The instantaneous measured and estimated fuel consumption rates were compared by running the test vehicles on the Arterial LOS (Level of Service) A cycle, as illustrated in Figure 10. Superimposed on the figure are the VT-CPFM-1 model estimates, which were computed using each of the vehicle-specific parameters. As illustrated in Figure 10, the predicted fuel consumption rates generally follow the peaks and valleys of the measured data and demonstrate a good agreement with field measurements. Specifically, the test vehicle consumed 0.67 liters of fuel while the model estimated 0.78 liters of fuel, which is an error of 16 percent. While it appears that the proposed model overestimates fuel consumption rates for the cycle, the model predictions follow the field-collected fuel measurements with high correlation coefficients (98%).

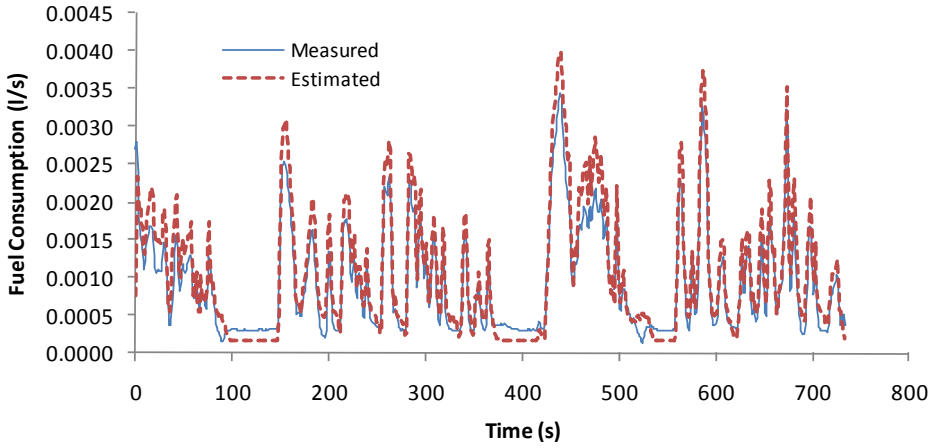

Figure 10. Validation of fuel consumption model

4.2 Vehicle Powertrain Model

There have been many studies on the modeling of vehicle engines and controls specifically for engine design, analysis, and control. While these models are sufficient for their intended purposes, they are not adequate for use in microscopic traffic simulation software for two reasons. Typical engine models are computationally intensive and cannot be integrated within car-following, lane-changing, and gap acceptance algorithms, which are critical for traffic simulation models. Second, these models require proprietary parameters that are difficult to obtain and in some instances require gathering field data for a vehicle's entire envelope of operation. The development of a vehicle powertrain model that can be utilized for traffic simulation modeling is a new challenge for traffic engineers.

The research team has developed a powertrain model that is used within the context of this approach. The powertrain model uses driver throttle input to compute the engine speed and power and finally compute the vehicle acceleration, speed, and position. The model can also be calibrated using vehicle parameters that are publicly available without the need for field data collection. **Figure 11** illustrates the basic concepts of the powertrain model. Using the driver's throttle input (f_p), the engine speed (w) is computed using a simple regression model that was developed in an earlier publication using field observations of engine speed and throttle level.[64] The engine power and torque is then computed considering an upper bound parabolic function that was developed by Ni and Henclewood ($P_{max}(w)$).[65] The actual power available is estimated as the proportion of the maximum power considering a linear transformation from throttle position to the proportion of maximum power available (i.e., $P(w) = f_p \times P_{max}(w)$). In the case of a manual transmission system, the gear selection is made directly using the engine speed. Alternatively, in the case of an automatic transmission system, the torque converter is modeled to compute an engine speed and torque generated by the torque converter.[66] The vehicle acceleration is then computed considering a point mass vehicle dynamics model as was presented earlier. The vehicle speed and position are estimated by solving

the second-order differential equation. The specifics of each of the components of the vehicle powertrain models are described in Rakha et al.[64]

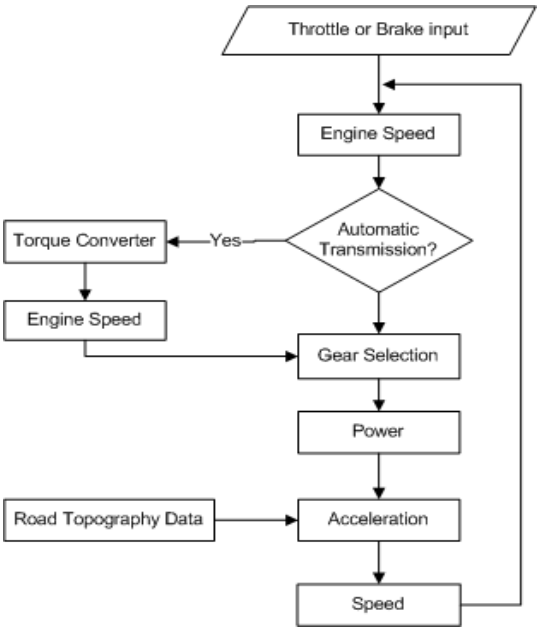

Figure 11. Proposed powertrain model structure

Figure 12 illustrates the measured instantaneous vehicle power rate of a vehicle in the southbound study section of I-81 and the estimated power from the powertrain model. The vehicle driving-related data were collected using an OBD II data logger. Cruise control operation data were utilized for this validation section. The target speed was set to 104 km/h (65 mi/h). The results clearly demonstrate a good agreement between the instantaneous power estimates and field measurements. As illustrated in the figures, the predicted power generally follows the peaks and valleys of the measured data except for a few high power points. Specifically, the 2007 Chevy Malibu generated 13,297 kW of power along the southbound section of I-81, while the proposed model estimated 13,871 kW of power using the same speed and road topographic profile, which is an error of approximately 4.3 percent. The figure also illustrates the instantaneous measured and estimated fuel consumption rates, which were compared by simulating the test vehicle (2007 Chevy Malibu) on the southbound section of I-81. Superimposed on the figures are the fuel consumption model (VT-CPFM-1 model) estimates, which were computed using the vehicle-specific parameters. The figure indicates a close match between predicted and measured fuel consumption levels and demonstrates a good agreement with field measurements. While it appears that the proposed model overestimates some fuel consumption rates and underestimates others, in general the model predictions follow the field-collected fuel measurements. Specifically, in the case of the southbound trip, the test vehicle consumed 1.33 liters of fuel while the model estimated 1.40 liters of fuel, which is an error of 5.5 percent.

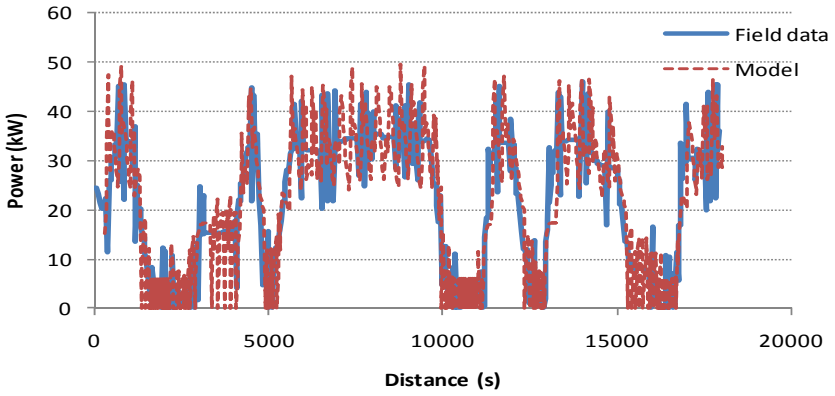

(a) Instantaneous Power (I-81)

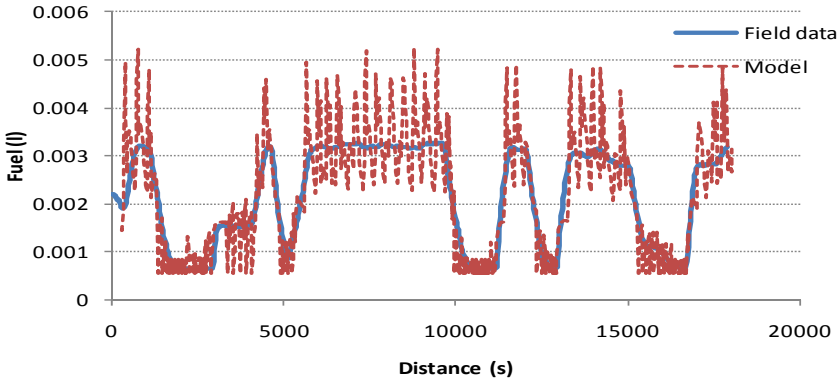

(b) Instantaneous Fuel (I-81)

Figure 12. Instantaneous powertrain and fuel model validation (2007 Chevy Malibu)

4.3 Predictive Eco-Cruise Control Algorithm Logic

The research team developed a predictive ECC system that generates optimal vehicle controls using topographic data. The study employs the operational concept of this predictive ECC system to build the proposed system. The system optimizes the vehicle controls in advance using a widely used dynamic programming (DP) implementation of Dijkstra's shortest path algorithm.

There are three system parameters used, namely: the stage length (d_s), the look-ahead distance (d_o), and the optimization implementation distance (d_f), as illustrated in **Figure 13**. The stage length (d_f), the first parameter, is the unit of discretization for solving the problem. In other words, the estimated vehicle optimal speed remains constant for the duration of a stage. The look-ahead distance (d_o), the second parameter, is the distance for which the optimization is performed. Finally, the optimization implementation distance (d_f), the last parameter, is the distance for which the optimized plan is implemented.

For example, assume that a driver plans a 5-km long trip and defines the stage length (d_s), the look-ahead distance, and the optimization implementation distance (d_f) as 100 m, 1 km, and 500 m, respectively. First, the system calculates the optimal vehicle speed for a look-ahead distance, 1 km section, from 0 m to 1000 m. Since the stage length (d_s) is 100 m, the optimal speed is estimated for every 100 m section. The estimated vehicle optimal speed remains constant for 100 m. Since the optimization implementation distance (d_f) is 500 m, when vehicle arrives at 500m the system repeats the optimization looking ahead from 500 m to 1500 m. Then the optimization is carried out every 500 m using the road profile over the next 1 km section.

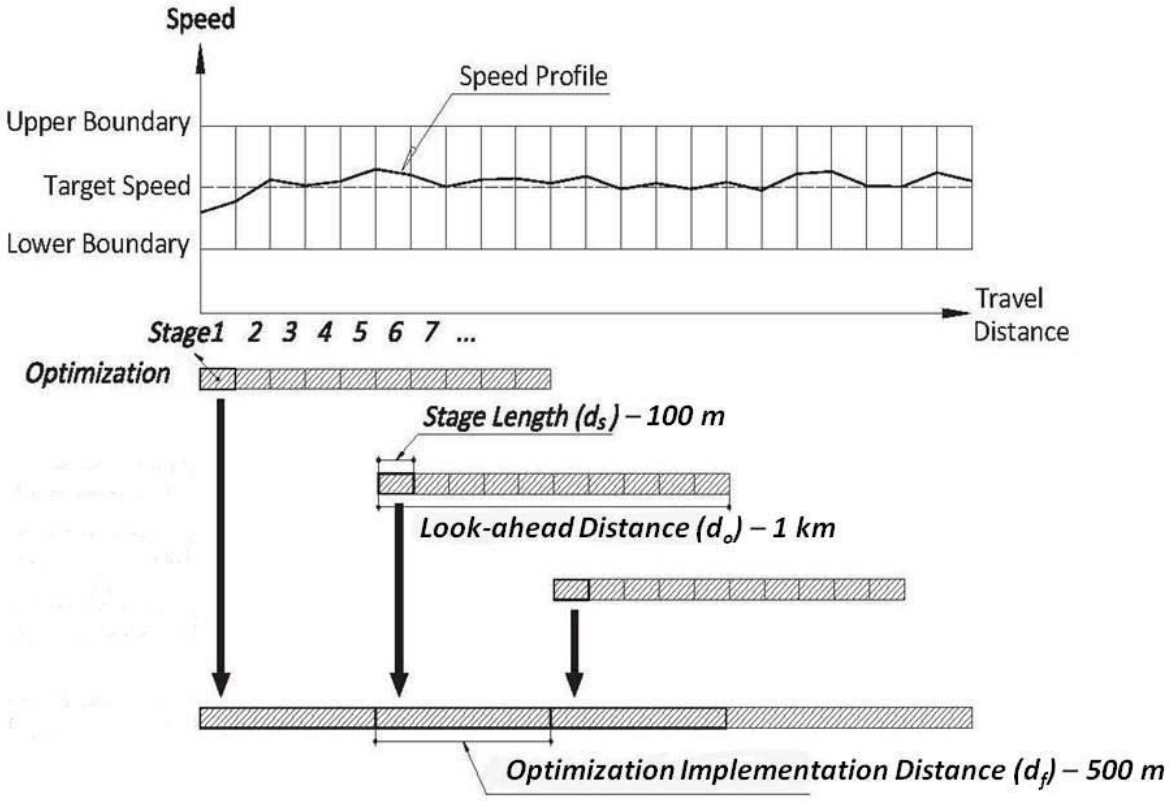

Figure 13. Proposed optimization methods

An optimization can be divided into three steps. The search space is defined in the first step using the powertrain module, which defines the space of speed and gears that the vehicle is physically able to achieve under the given topographical information and vehicle performance. For the optimization in the second step, the defined continuous search space is discretized for the speed and gear levels. Each of the discretized points represents a state that consists of a speed and a gear combination. Transition from a state at the beginning of stage *i* to a state at the end of stage *i* represents changes in the vehicle speed and gear over the stage *i*. In this step, all the transitions are evaluated using a cost function, as shown in the equation in **Figure 14**, that computes the fuel consumption rates and other penalties:

$$Cost = w_1 FC_{(v_0, v_1)} + w_2 \mid v_1 - v_{ref} \mid FC_{(v_{ref})} + w_3 \mid g_1 - g_0 \mid FC_{(v_{ref})}$$

Figure 14. Cost function

where w_1 is the weight factor for fuel consumption, w_2 is the weight factor for the deviation from the target speed, w_3 is the weight factor for gear change, v_0 is the initial speed, v_1 is the final speed, v_{ref} is the target speed, g_0 is the initial gear, g_1 is the final gear, $FC_{(v0,v1)}$ is the fuel consumption to travel from v_0 to v_1 over a stage length, and $FC_{(vref)}$ is the fuel consumption at v_{ref} over a stage length. Finally, the module finds an optimal control plan using either Dijkstra's shortest path or a heuristic algorithm that was developed by the research team to enhance the computational efficiency of the algorithm.

4.4 Proposed Car-Following Algorithm

Car-following models assume that there is a relationship between the spacing between the subject and lead vehicle and the speed of the following vehicle in a range of inter-vehicle spacings. The process of car-following is modeled as equations of motion under steady-state conditions plus a number of constraints that govern the behavior of vehicles while moving from one steady state to another (decelerating and accelerating). The exploratory study used the Rakha-Pasumarthy-Adjerid (RPA) car-following model.

4.4.1 Steady-State Modeling

This study would consider the use of the Van Aerde steady-state car-following model, which is a nonlinear, single-regime functional form. The original model, shown in the equation in **Figure 15**, was proposed in Van Aerde[67] and in Van Aerde and Rakha[68,69]:

$$s_n(t + \Delta t) = c_1 + c_3 u_n(t + \Delta t) + \frac{c_2}{u_f - u_n(t + \Delta t)}$$

Figure 15. Van Aerde steady-state car-following model

where $s_n(t)$ is vehicle spacing at time t, $u_n(t)$ is speed of vehicle n at time t (km/h), u_f is free-flow speed (km/h), Δt is length of time interval, c_1 is fixed distance headway constant (km), c_2 is the first variable headway constant (km^2/h), and c_3 is the second variable distance headway constant (h).

Rakha demonstrated that the c_1, c_2, and c_3 parameters can be computed as shown in the equation in **Figure 16**.[70] To ensure that the speed estimates are realistic, the square root term should be positive. This is achieved if the model parameters satisfy the condition of the equation in **Figure 17**.[70]

$$c_1 = \frac{u_f}{k_j u_c^2}(2u_c - u_f); c_2 = \frac{u_f}{k_j u_c^2}(u_f - u_c)^2; c_3 = \left(\frac{1}{q_c} - \frac{u_f}{k_j u_c^2}\right)$$

Figure 16. c_1, c_2, and c_3 parameters

.

$$q_c \leq \frac{k_j u_c u_f}{2u_f - u_c}$$

Figure 17. Speed estimate parameters

where u_c is speed-at-capacity (km/h), k_j is jam density (veh/km), and q_c is the capacity (veh/h).

Typically the vehicle speed or the acceleration level is considered as the control variable. Consequently, the vehicle speed is estimated as shown in the equation in :**Figure 18**

$$u_n(t + \Delta t) = \frac{-c_1 + c_3 u_f + s_n(t + \Delta t) - \sqrt{[c_1 - c_3 u_f - s_n(t + \Delta t)]^2 - 4c_3[s_n(t + \Delta t)u_f - c_1 u_f - c_2]}}{2c_3}$$

Figure 18. Vehicle speed estimate

where $s_n(t)$ is the predicted vehicle spacing at time t considering that vehicle n continues at its current speed, where $s_n(t + \Delta t) = s_n(t) + [u_{n-1}(t) - u_n(t)]\Delta t + 0.5a_{n-1}(t)\Delta t^2$, and where $a_n(t)$ is the acceleration of vehicle n at time t.

4.4.2 Collision Avoidance Modeling

In the case that the following vehicle is traveling at a higher speed than the lead vehicle (non-steady state conditions) the vehicle spacing should be sufficient to allow the following vehicle (vehicle n) to avoid a collision with the lead vehicle (vehicle $n - 1$). This deceleration level of the following vehicle is assumed to be equal to $\mu f_b \eta_b g$, where μ is the coefficient of roadway friction, f_b is the driver brake pedal input [0,1], η_b is the brake efficiency [0,1], and g is the gravitational acceleration (9.8067 m/s^2). The resulting minimum vehicle spacing and the vehicle speed can be computed using the equations in **Figure 19** and **Figure 20**, respectively.

$$s_n(t + \Delta t) = \frac{1}{k_j} + \frac{u_n(t + \Delta t)^2 - u_{n-1}(t + \Delta t)^2}{25920 m f_b h_b g}$$

Figure 19. Minimum vehicle spacing

$$u_n(t + \Delta t) = \sqrt{u_{n-1}(t + \Delta t)^2 + 25920 m f_b h_b g \left(s_n(t + \Delta t) - \frac{1}{k_j} \right)}$$

Figure 20. Vehicle speed

4.4.3 Vehicle Acceleration Modeling

Vehicle acceleration can be modeled in two different ways: using a vehicle dynamics model or a vehicle powertrain model. The vehicle dynamics approach approximates the vehicle as a point mass and ignores any gear-shifting effects on vehicle modeling. A vehicle powertrain approach requires more computations because it models the vehicle gearbox. This study uses the vehicle dynamics model.

Vehicle acceleration may be modeled considering the vehicle as a point mass and only considering the various forces acting on the vehicle. Vehicle dynamics models compute the maximum vehicle acceleration levels from the resultant forces acting on a vehicle (mainly vehicle tractive forces, which are a function of the driver throttle input and resistance forces).

The vehicle tractive effort can be computed using Equation (16). Rakha and Lucic introduced the β factor into the equation in **Figure 21** to account for the effects of gear shifts at low traveling speeds when trucks are accelerating.(71) This factor is set to 1.0 for light-duty vehicles.(72) The $f_p(t)$ factor models the driver throttle input level and ranges from 0.0 to 1.0. The vehicle resistance force is calculated as the sum of the aerodynamic, rolling, and grade resistance forces acting on the vehicle,(71,73) as demonstrated in the equation in **Figure 22**.

$$F_n(t) = \min\left(3600 f_p(t)\, b\, h_d \frac{P_n}{u_n(t)}, m_n' g \mu\right)$$

Figure 21. Vehicle tractive effort

$$R_n(t) = \frac{r}{25.92} C_d C_h A_f u_n(t)^2 + m_n g \frac{c_{r0}}{1000}\left(c_{r1} u_n(t) + c_{r2}\right) + mgG(t)$$

Figure 22. Vehicle resistance force

where $f_p(t)$ is the driver throttle input at time t [0,1] (unitless); β is the gear reduction factor (unitless); η_d is the driveline efficiency (unitless); P is the vehicle power (kW); m'_n is the mass of vehicle n on its tractive axle (kg); g is the gravitational acceleration (9.8067 m/s^2); μ is the coefficient of road adhesion or the coefficient of friction (unitless); ρ is the air density at sea level and a temperature of 15°C (1.2256 kg/m^3); C_d is the vehicle drag coefficient (unitless), typically 0.30; C_h is the altitude correction factor (unitless), which is computed as C_h=1-0.085H where H is the altitude (km); A_f is the vehicle frontal area (m^2); c_{r0} is the rolling resistance constant (unitless); c_{r1} is the rolling resistance constant (h/km); c_{r2} is the rolling resistance constant (unitless); m_n is the total vehicle mass (kg); and $G(t)$ is the roadway grade at instant t (unitless). The rolling resistance parameters vary as a function of the road surface type, road condition, and vehicle tires.(73) Generally, radial tires provide a resistance that is 25 percent less than that of bias ply tires. Typical values of vehicle frontal areas for different vehicle types and typical drag coefficients are provided in the Rakha et al.(73) Typical values for the

coefficient of roadway adhesion and the rolling resistance coefficients are provided in in Rakha and Lucic[71] and Rakha et al.[73]

The vehicle acceleration is calculated as a ratio of the difference between the tractive and resistance forces divided by the vehicle mass (i.e., $a=(F-R)/m$). The vehicle speed and position at $t + \Delta t$ is then computed using a first-order Euler approximation, as demonstrated in the equations in **Figure 23** and **Figure 24**.

$$u_n(t + \Delta t) = u_n(t) + 3.6\frac{F_n(t) - R_n(t)}{m}\Delta t$$

Figure 23. Vehicle speed

$$x_n(t + \Delta t) = x_n(t) + u_n(t)\Delta t$$

Figure 24. Vehicle position

5 Proposed Algorithm

The research proposes an Eco-Driving application to reduce fuel consumption and GHG emissions, as illustrated in **Figure 25**. The model starts with driver input of a target speed range and following headway. Alternatively, the system can locate the vehicle on a high-resolution digital map to identify the desired speed based on the roadway speed limit. The driver can then set a range for the desired speed. Using the road's topographic information, the system estimates the optimal speed profile that minimizes the vehicle fuel consumption within the target speed range. The optimal control estimates the throttle position and brake level that generates the desired speed profile while maintaining a safe following headway and spacing between the subject vehicle and a vehicle ahead of it. The model utilizes the vehicle powertrain model that was described earlier to compute the feasible gear and speed range for use in the optimization algorithm.

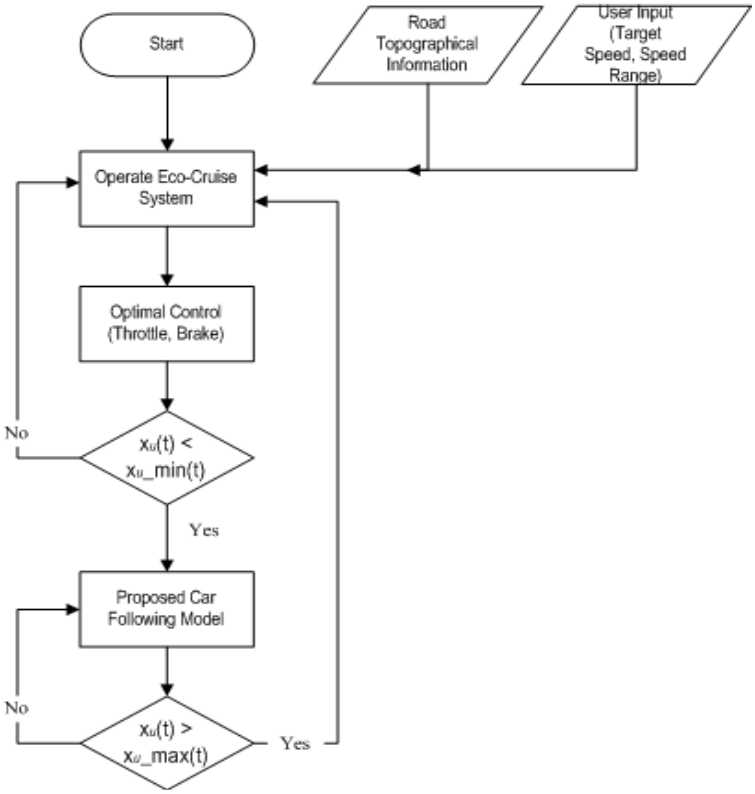

Figure 25. Proposed Eco-Driving logics

5.1 Model Algorithm

The proposed logic can be summarized as follows:

1. If the spacing between the subject and lead vehicle is beyond the car-following threshold, proceed to step 3. Otherwise, proceed to step 2.
2. Estimate the maximum vehicle acceleration at instant *t* based on the steady-state car-following model and collision avoidance constraints. Considering the Van Aerde functional form, the first step entails computing the maximum speed at $t+\Delta t$ using the equation in **Figure 26**. The maximum acceleration is then computed using the equation in **Figure 27**, and the maximum speed at the end of the first stage (position x_t+d_s) can then be computed using the equation in **Figure 28**. Proceed to step 4.

$$\hat{u}_n(t+\Delta t) = \min\left\{\frac{-c_1 + c_3 u_f + v_n(t) - \sqrt{[c_1 - c_3 u_f - v_n(t)]^2 - 4c_3[v_n(t)u_f - c_1 u_f - c_2]}}{2c_3},\ \sqrt{u_{n-1}(t+\Delta t)^2 + 25920 m f_b h_b g\left(s_n(t) - \frac{1}{k_j}\right)}\right\}$$

Figure 26. Van Aerde functional form

$$\hat{a}_n(t) = \frac{\hat{u}_n(t + \Delta t) - u_n(t)}{\Delta t}$$

Figure 27. Maximum acceleration

$$\hat{u}_n(x_t + d_s) = \sqrt{u_n(x_t)^2 + 2\hat{a}_n(t)d_s}$$

Figure 28. Maximum speed at the end of the first stage

3. Using the DP algorithm described earlier, the optimal vehicle speed trajectory over the look-ahead distance (d_o) is estimated considering a spatial discretization of d_s (stage length). The maximum car-following speed constraint that was computed in step 2 is considered in identifying the search space of stage 1.
4. Move the vehicle and then go back to step 1 at the conclusion of time step Δt. Otherwise, end the simulation at $t=T$.

5.2 Model Calibration Issues

The calibration of the proposed model entails calibrating the four steady-state traffic stream parameters, the maximum comfortable braking level, the various vehicle and powertrain parameters, and the optimization parameters.

The steady-state car-following model requires the calibration of four parameters: free-flow speed, speed-at-capacity, capacity, and jam density. The speed-at-capacity can be set to equal the free-flow speed. This results in a linear car-following model, also known as the Pipes model. The free-flow speed, as was mentioned earlier, can be derived if the vehicle location is identified on a digital map. The user can then set a free-flow speed range to control the vehicle instead of setting a preset, single free-flow speed. The capacity is computed as the inverse of the adaptive cruise control headway setting (h_c) of the ACC system ($q_c = 3{,}600/h_c$). The jam density can be estimated using the vehicle length (L_v) and the spacing between the front and rear bumpers of vehicles in a queue (b_j) ($k_j = 1000/(L_v + b_j)$). Typically, b_j ranges from 0.5 to 1.5 m.

The maximum comfortable deceleration level is a function of the roadway surface condition, the type of vehicle tires, the type of vehicle braking system (ABS or no ABS), and the driver input. Typical values are in the range of 0.6 g.

Table 1 summarizes some sample vehicle powertrain parameters. Below is a description of each of the parameters listed in the table and how the values can be obtained:

- **Vehicle Engine Power (P, in kW)**: The engine power can be obtained from the vehicle specifications on automotive manufacturer Web sites.
- **Engine Efficiency**: Power losses in the engine due to internal friction and other factors generally account for between 5 and 10 percent of the engine losses for light-duty vehicles.(66)

- **Vehicle Mass (kg)**: Vehicle mass is an important parameter in the model because it determines the force required to accelerate a vehicle. Vehicle weights can be obtained from automotive manufacturer Web sites.
- **Percentage of Vehicle Mass on the Tractive Axle (m_{ta}/m)**: This can be obtained from manufacturer Web sites, measured in the field, or assumed. In the case of light-duty vehicles, typical values for front-wheel-drive vehicles are in the range of 50 to 65 percent, reflective of the high weight of the engine sitting on top of the axle. For rear-wheel-drive vehicles, the mass on the tractive axle typically ranges between 35 and 50 percent of the total mass.
- **Frontal Area (A_f, in m^2)**: The frontal area of the vehicle can be approximated as the product of 85 percent of the height and the width of the vehicle. Vehicle height and width are available from automotive manufacturers.
- **Air Drag Coefficient (C_d)**: The air drag coefficient is typically available on automotive Web sites. If not, these values may be assumed. Typical values for light-duty vehicles range from 0.30 to 0.35, depending on the aerodynamic features of the vehicle.

Table 1. Summary of light-duty test vehicle characteristics

Vehicle	EPA Class	P (kW)	Mass (kg)	m_{ta}/m (%)	A_f (m^2)	C_d
1996 Geo Metro Hatchback	Subcompact	41.0	1130	0.380	1.88	0.34
1995 Acura Integra SE		105.9	1670	0.515	1.94	0.32
1995 Saturn SL	Compact	92.5	1240	0.560	1.95	0.33
2001 Mazda Protégé LX 2.0		97.0	1610	0.525	2.04	0.34
2001 Plymouth Neon		98.5	1650	0.495	2.07	0.36
1998 Ford Taurus	Midsize	108.2	1970	0.575	2.26	0.30
1998 Honda Accord		111.9	1770	0.610	2.12	0.34
1995 BMW 740I		210.4	2370	0.515	2.27	0.32
1995 Dodge Intrepid	Large	120.1	2040	0.535	2.30	0.31
1999 Ford Crown Victoria		149.2	2300	0.590	2.44	0.34
1998 Ford Windstar LX	Minivan	149.2	2270	0.550	2.73	0.40
1995 Chevy S-10	Pickup	145.47	1930	0.605	2.31	0.45
1995 Chevy Blazer	SUV	145.47	2310	0.560	2.49	0.45

6 Simulation Results

This section describes the simulation results of the proposed Eco-Driving system. The computer simulation software, MATLAB, was utilized to develop and evaluate the performance of the proposed models. Key input variables for the proposed system include the car-following spacing threshold; the car-following model parameters such as the free-flow speed, jam density, speed-at-capacity, and capacity parameters; vehicle data including powertrain-related data and fuel economy data; roadway topography data; real-time location data; and lead vehicle location data (or spacing data). In the simulated Eco-Driving system, the subject vehicle alternatively operated in either the predictive eco-cruise control mode or, if the spacing between the subject and lead vehicle was within the car-following threshold, in the car-following mode. The following sections describe the various sensitivity tests performed to study the impact of the proposed Eco-Driving system.

6.1 Different Car-Following Thresholds

ECC systems optimize vehicle speed to minimize fuel consumption and GHG emissions. However, the typical ECC system assumes that the ECC vehicle does not interact with other vehicles, requiring drivers to operate ECC vehicles with caution to avoid collisions. The proposed ECC system integrates a car-following logic that includes a collision avoidance algorithm to improve safety while at the same time minimize the vehicle fuel consumption level.

This section describes the impacts of using different car-following thresholds and parameters on the proposed system performance. As described earlier, the proposed system operates either in the ECC or car-following mode. The user-defined car-following threshold significantly affects the performance of the system. The research investigates three car-following thresholds: 100 m, 50 m, and 30 m.

Figure 29 illustrates the speed profile of a lead vehicle and altitude data along the study section. The research used a 22-km section of I-81in southwestern Virginia, between mileposts 132 (Roanoke, Virginia) and 118 (Christiansburg, Virginia), which ranges from an elevation of 350 to 629 m above mean sea level. The maximum grade along the study section is 4 percent, and the maximum downhill grade is -5 percent, with an average grade of 0.6 percent.

The speed data were collected from the lead vehicle, a 2007 Chevy Malibu, using an OBD II data logger that also collected GPS signals. The drivers were instructed to maintain the target speed of 104 km/h (65 mi/h) without using cruise control. However, the figure shows that manual driving causes significant speed variations due to various roadway conditions.

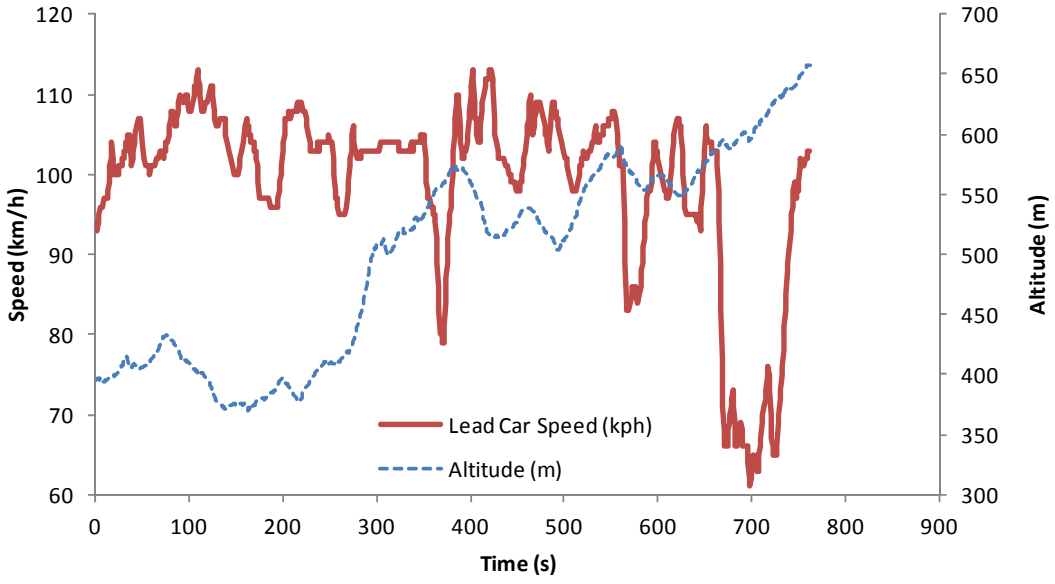

Figure 29. Lead vehicle speed profile

Figure 30 illustrates the proposed car-following operation on the study section of I-81. The test vehicle was a 2011 Toyota Camry, which has a 2.4-L engine and 21 and 31 miles per gallon (mpg) for city and highway fuel economy, respectively. As illustrated in the figure, the test vehicle followed the lead vehicle almost exactly, with an average vehicle spacing of 50 m. When the lead vehicle slowed, the proposed car-following algorithm reduced the spacing. The test vehicle generated a fuel economy of 13.5 mpg on the study section, which is significantly lower than the posted fuel economy data due to the multiple major roadway upgrade sections.

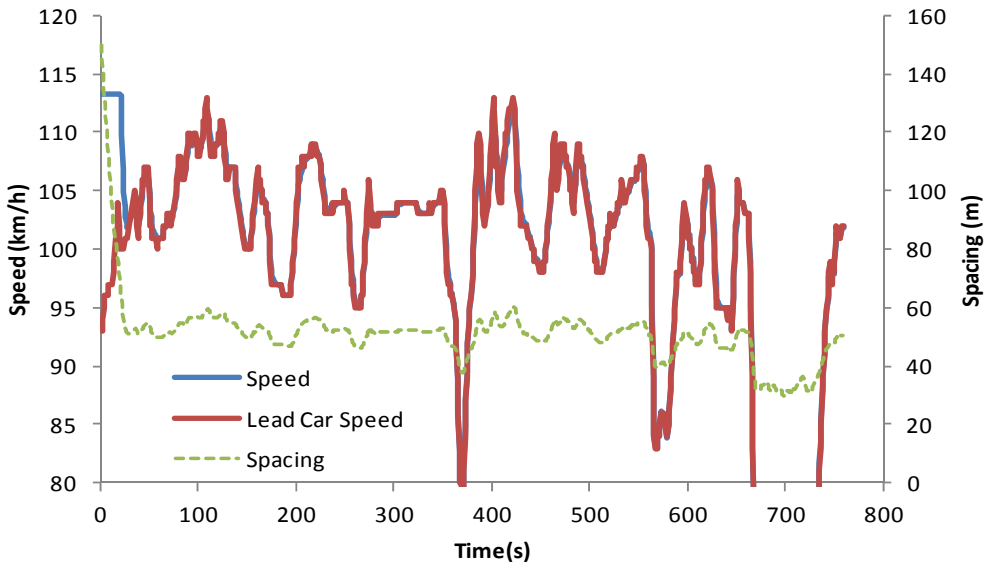

Figure 30. Car-following-only operation speed and spacing profiles

Figure 31 illustrates the speed profile of ECC operation on the study section of I-81. A vehicle trip using the test vehicle and roadway grade profiles was simulated with the predictive ECC system at a target speed of 104 km/h (65 mi/h). For the predictive system, the vehicle was allowed to vary its speed by ± 8 km/h (± 5 mi/h) from the target speed. As shown in the figure, the predictive ECC system varied the vehicle speed using the topographical information. The results clearly illustrate that the test vehicle was controlled to maintain the lowest speed within the speed window on the uphill sections when the predictive control system was engaged. Furthermore, the speed was highest on the downhill sections because the predictive system attempted to maximize the use of gravitational energy. The test vehicle generated a fuel economy of 24.6 mpg on the study section, which is significantly greater than in the car-following-only operation. Specifically, the ECC operation increased the fuel economy of the test vehicle, a 2011 Toyota Camry, by up to 82 percent compared to the car-following-only mode of operation.

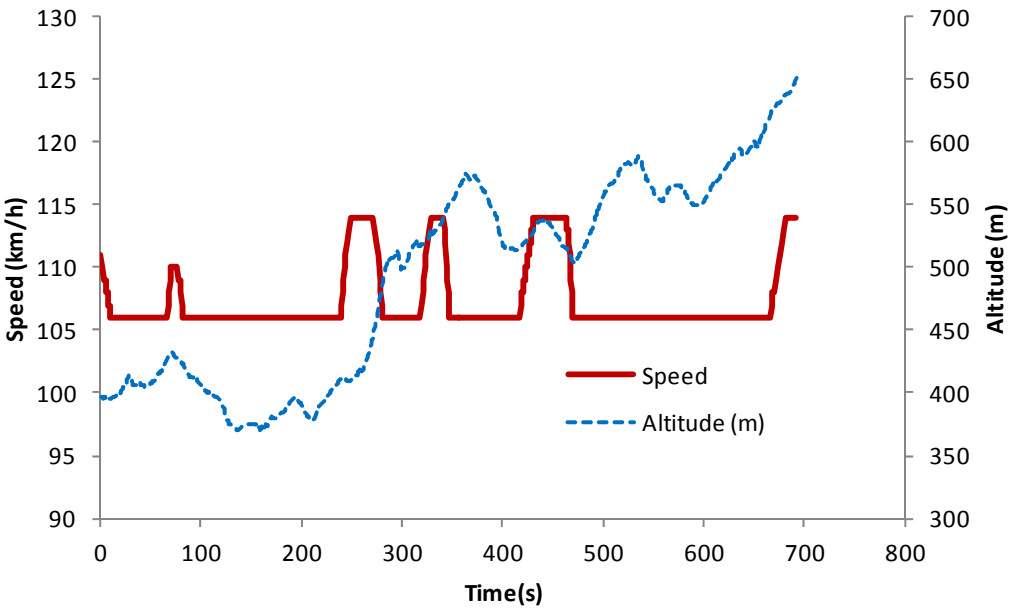

Figure 31. Eco-cruise control operation, Toyota Camry

Figure 32 illustrates the simulated speed profiles of different car-following thresholds. The 2011 Toyota Camry was utilized for this simulation. As shown, the car-following threshold setting significantly affects the vehicle speed profiles. For the 100-m car-following threshold, the test vehicle is mostly engaged in the car-following mode (98.7 percent of the trip) and the speed profile is almost identical to that of the lead vehicle. During the trip, the test vehicle consumed 3.7 L of fuel, with a fuel economy of 13.5 mpg over the trip. The figure also illustrates the speed profile of the 50-m car-following threshold simulation run. The vehicle speed profile is notably different from that of the 100-m car-following threshold. When the test vehicle adopts the 50-m car-following threshold, the speed profile of the test vehicle differs from that of the lead vehicle but finds an optimal speed profile. The simulation results demonstrate that the test vehicle operates in the ECC mode for 85 percent of the trip and engages in the car-following mode of operation for only 15 percent of the trip. Also, when using the 50-m car-following threshold, the test vehicle improves its fuel economy to 16.0 mpg, which is an 18 percent improvement from both the car-following-only mode and the 100-m car-following threshold mode. The figure also illustrates the speed profile of the 30-m car-following threshold. The simulation results show that the test vehicle undergoes two significant speed reductions at times 75 s and 485 s. These were caused by the spacing between the lead and subject vehicle falling below the collision avoidance distance. For the 30-m car-following threshold case, the test vehicle utilizes the ECC mode for most of the trip (97 percent) and improves its fuel economy to 20.5 mpg.

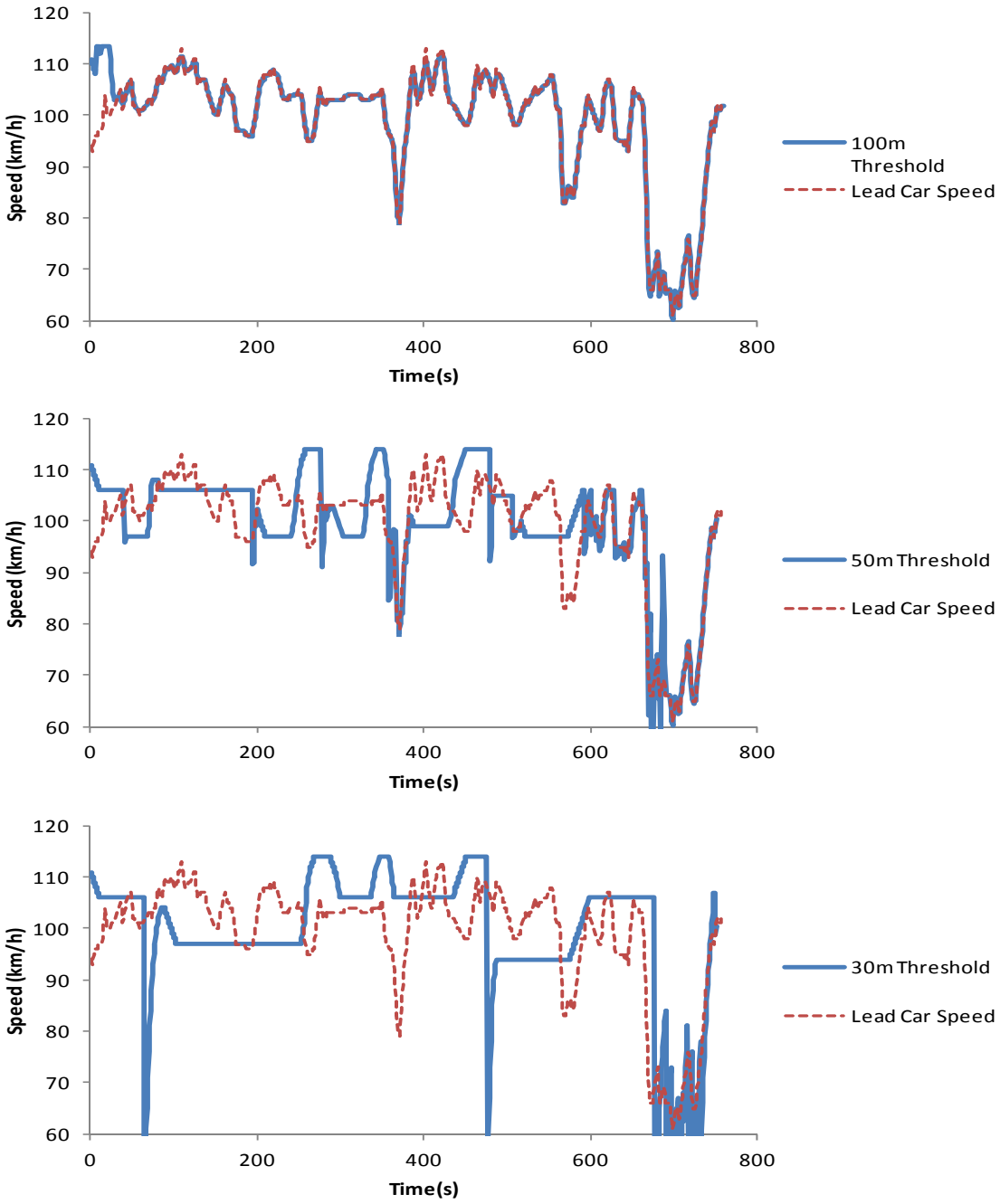

Figure 32. Different car-following thresholds, Toyota Camry

Figure 33 and **Figure 34** illustrate simulation results of using different car-following thresholds for a 2008 Chevy Tahoe and a 2008 Chevy Malibu Hybrid. The figures demonstrate that the speed profiles of test vehicles show similar patterns for each car-following threshold. For instance, when the 100-m car-following threshold is used, all test vehicles operate mostly in the car-following mode, up to 99 percent of the trip. However, for the 50-m and 30-m car-following thresholds, the test vehicles generally operate in the ECC mode. In addition, for the 30-m car-following threshold, the test

vehicles maintain constant speeds for longer periods of time than for the 50-m car-following threshold.

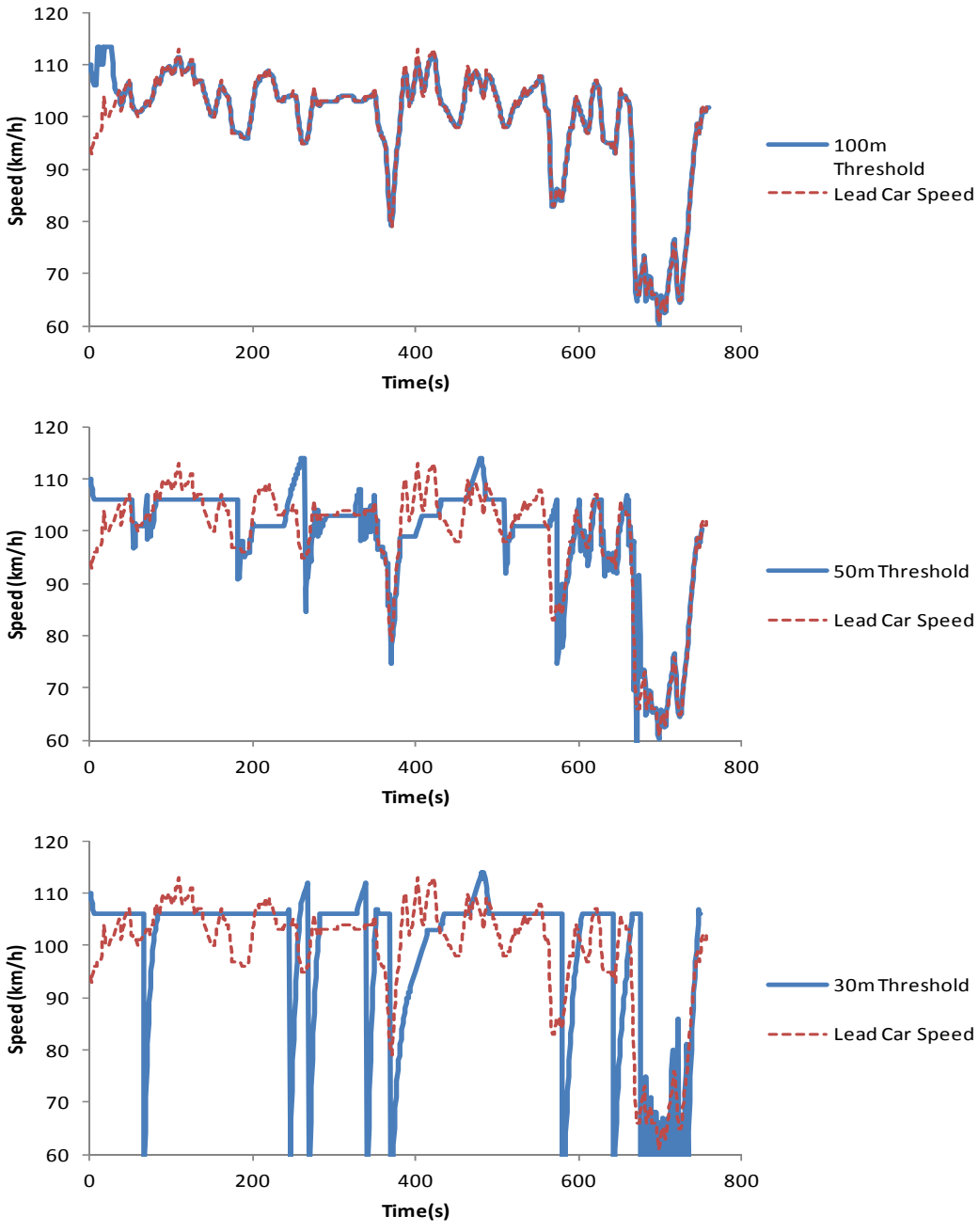

Figure 33. Different car-following thresholds, Chevy Tahoe

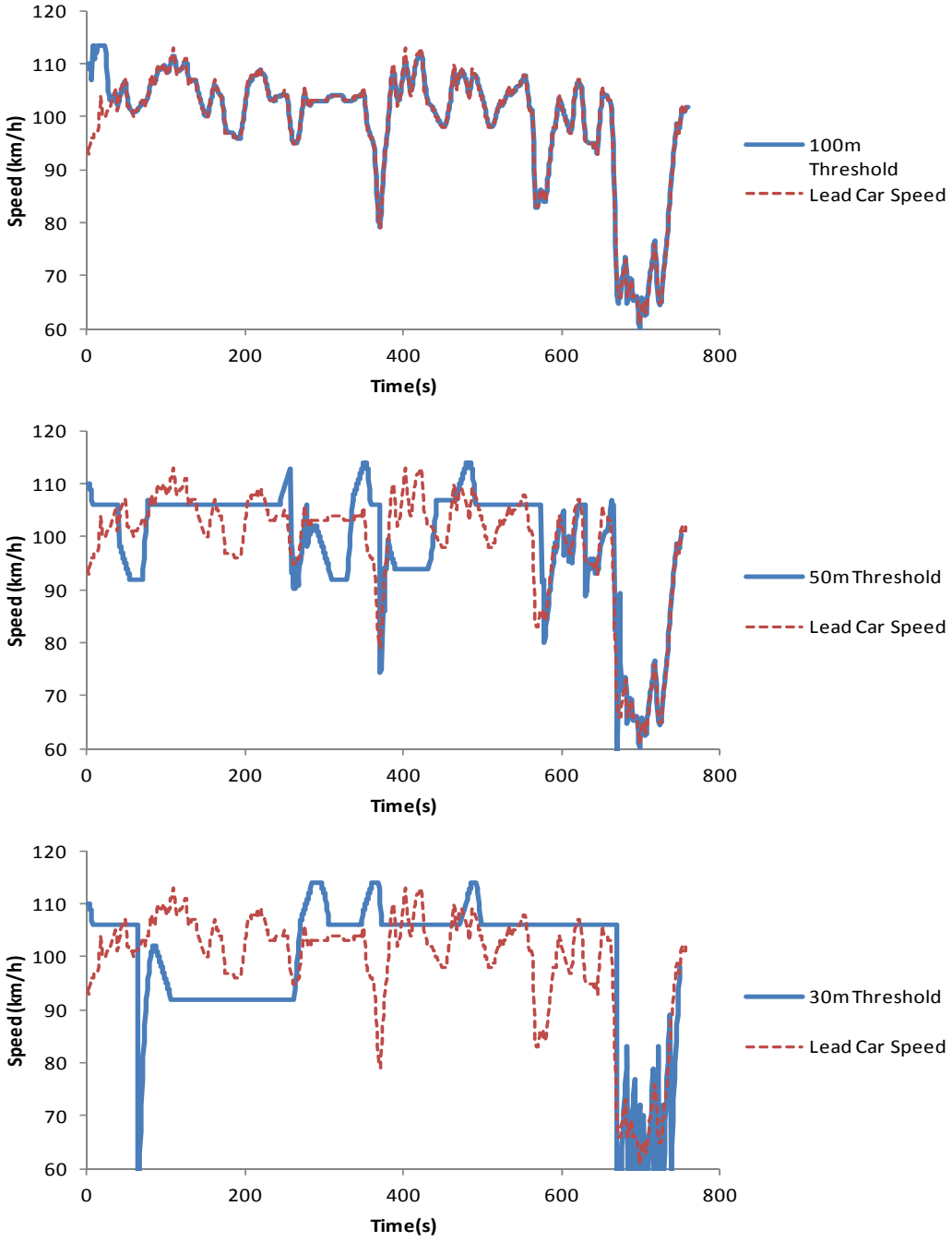

Figure 34. Different car-following thresholds, Malibu Hybrid

Table 2 summarizes the simulation results, which demonstrate that ECC-only operation can significantly improve fuel efficiency compared to car-following mode of operation. Furthermore, as described earlier, the test vehicles attained the best fuel economy while interacting with the lead vehicles on the test road for the 30-m car-following threshold.

Based on the simulation runs, the proposed system improves the fuel efficiency of the Toyota Camry, Chevy Tahoe, and Malibu Hybrid by up to 51, 21, and 31 percent, respectively. In conclusion, the results demonstrate that the proposed Eco-Driving system can significantly improve vehicle fuel economy on the tested roadway section.

Table 2. Summary of results

	2011 Camry	2008 Tahoe	2008 Malibu Hybrid
Car-following only	13.5 mpg	8.9 mpg	16.2 mpg
Eco-cruise only	24.6 mpg (82%)	14.3 mpg (60%)	25.4 mpg (57%)
100-m Following Threshold	13.5 mpg (-0.6%)	8.7 mpg (-2%)	16.1 mpg (-0.1%)
50-m Following Threshold	16.0 mpg (18%)	9.6 mpg (8%)	19.2 mpg (19%)
30-m Following Threshold	20.5 mpg (51%)	10.8 mpg (21%)	21.2 mpg (31%)

Figure 35 illustrates how different car-following threshold settings affect the spacing between the lead vehicle and the test vehicle. The shorter car-following threshold typically increases the inter-vehicle spacing while considerably improving fuel efficiency. The results demonstrate that when the Toyota Camry operates with the 30-m car-following threshold, the maximum spacing between the test vehicle and the lead vehicle increases to a maximum spacing of 450 m with an average spacing of 196 m for the entire trip. However, the 100-m and 50-m car-following thresholds reduce the average spacing to 50 m and 78 m, respectively, for the Toyota Camry. The figure also illustrates the spacing profiles of the Chevy Tahoe. While the maximum and average spacing values of the Chevy Tahoe are smaller than those of the Toyota Camry, the results demonstrate that the maximum spacing value (230 m) for the 30-m car-following threshold is relatively higher than is typically found in normal highway driving conditions. It should be noted that longer spacing between vehicles reduces the capacity of the road and also causes frequent lane changing and cut-in maneuvers. The next section investigates the potential for dynamic car-following scenarios to lessen the spacing between the lead and subject vehicles.

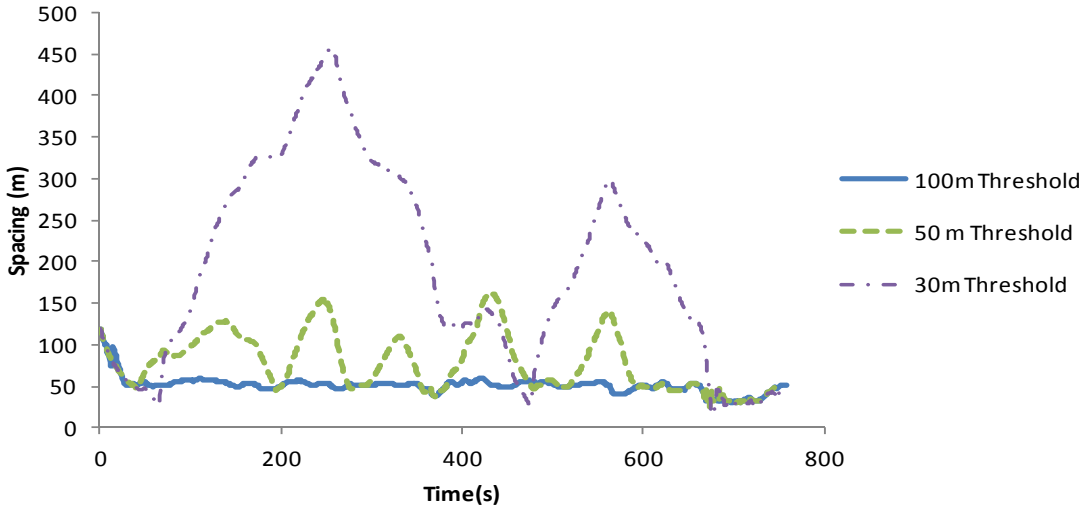

(a) Toyota Camry

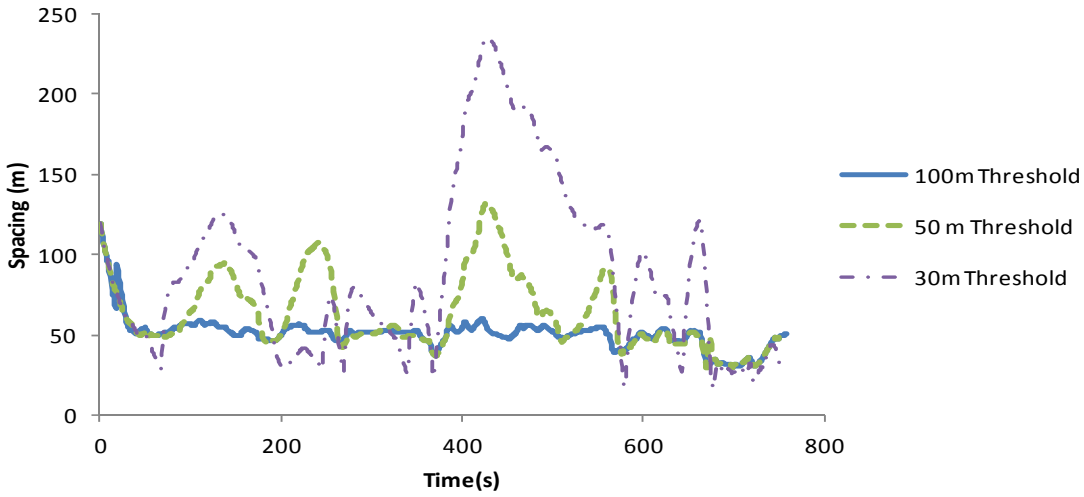

(b) Chevy Tahoe

Figure 35. Spacing of different car-following thresholds

6.2 Dynamic Car-Following Thresholds

This section investigates two dynamic car-following methods: dynamic threshold and dynamic threshold with maximum spacing limit. The dynamic threshold method increases the car-following threshold based on the vehicle spacing in order to minimize the vehicle spacing. As the vehicle spacing increases, the car-following threshold also increases, reverting the ECC operational mode to the car-following mode and reduce the vehicle spacing. Alternatively, if the spacing is reduced below the initial car-following threshold, the dynamic car-following threshold is set to the initial car-following threshold. Table 3 demonstrates the simulation results of using the dynamic car-following threshold. The results show that the dynamic car-following threshold method significantly reduces the average vehicle spacing without notably reducing the vehicle fuel economy. Specifically, the average vehicle spacing is reduced from 78 m to 54 m for the 50-m initial car-following threshold and from 196 m to 80 m with the 30-m initial car-following threshold. The results show that the dynamic car-following method slightly reduces fuel economy. In particular, the dynamic car-following threshold mode of operation decreases the vehicle fuel economy to 15.8 mpg and 18.3 mpg from 16 mpg and 20.5 mpg for the 50-m and 30-m fixed car-following thresholds, respectively.

Table 3. Dynamic car-following threshold fuel economy and average and maximum spacing, Toyota Camry

	Fixed Car- Following Threshold	Dynamic Car- Following Threshold	Dynamic Car-Following with Max Spacing Limit
Car-Following only	13.5 mpg		
100 m Following Threshold	13.5 mpg (50 m, 60 m)		
50 m Following Threshold	16.0 mpg (78 m, 161 m)	15.8 mpg (54 m, 179 m)	15.9 mpg (52 m, 183 m)
30 m Following Threshold	20.5 mpg (196 m, 457 m)	18.3 mpg (80 m, 289 m)	17.2 mpg (48 m, 133 m)

While the dynamic car-following threshold method significantly reduces the average spacing compared to the fixed car-following threshold method, the spacing values are relatively high for the 30-m initial car-following threshold, with 80 m and 289 m for average and maximum spacing values, respectively. To further reduce the spacing, the dynamic car-following method enforces a maximum spacing limit. If the spacing is greater than a pre-set maximum spacing limit, the ECC mode automatically switches to the car-following mode to reduce the vehicle spacing. **Figure 36** compares the speed profiles of the fixed 30-m car-following threshold and dynamic 30-m car-following threshold with a maximum spacing limit of 100 m. The test vehicle using the dynamic method with maximum spacing limit generally follows the lead vehicle without experiencing the sudden speed drops observed in the fixed car-following method. The new method also considerably reduces the average spacing from 196 m to 48 m for the 30-m initial car-following threshold. Furthermore, the maximum vehicle spacing is reduced from 457 m to 133 m. It is interesting to note that with the 50-m initial car-following threshold, the maximum spacing increases from 161 m to 183 m while the average spacing decreases from 78 m to 52 m.

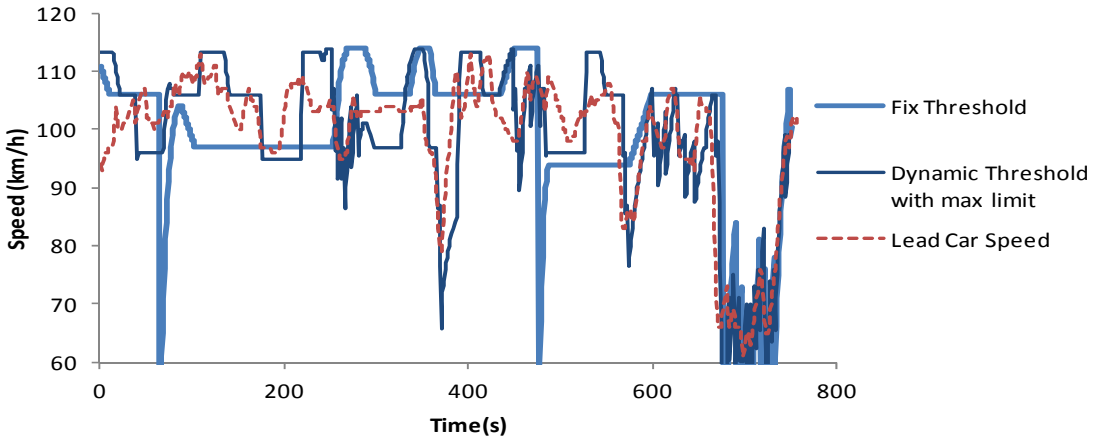

(a) Speed Profiles

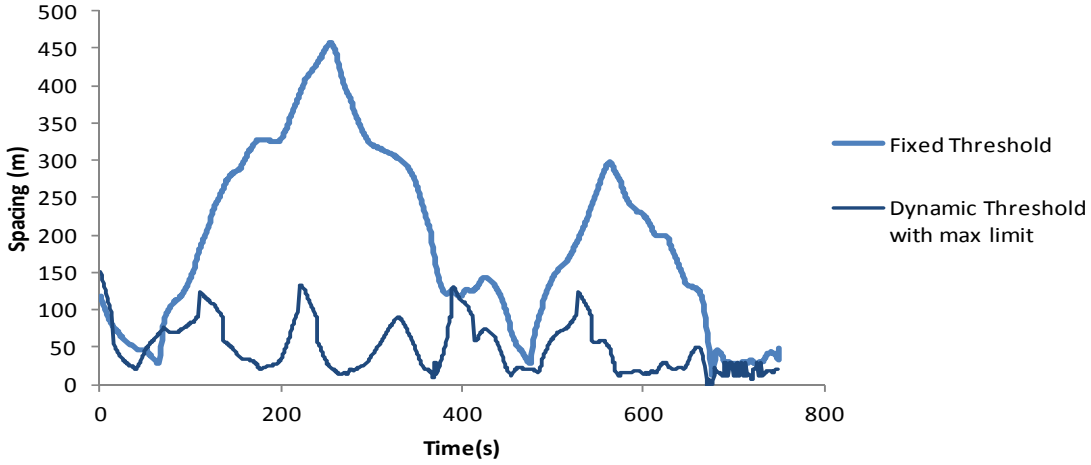

(b) Spacing

Figure 36. Dynamic car-following threshold results

Figure 36 illustrates the feasibility of using dynamic car-following thresholds instead of using a fixed car-following threshold. The study demonstrates that while the proposed Eco-Driving system significantly improves fuel economy, it also increases the spacing between a lead and the subject vehicles, particularly using the 30-m car-following threshold.

6.3 Impact of Throttle Levels on System Performance

Because power levels significantly affect fuel consumption rates, reducing the maximum throttle level can dramatically improve the overall fuel efficiency of the proposed system. This study investigated the impact of constraining the maximum throttle level to 60 and 40 percent to quantify the fuel saving benefits compared to 100 percent throttle level (Table 4).

Table 4. Summary of results for different throttle levels, Toyota Camry

	100% Throttle	60% Throttle	40% Throttle
Car-following only	13.5 mpg	15.8 mpg (16%)	20.2 mpg (49%)
Eco-cruise only	24.6 mpg (82%)		
100-m following threshold	13.5 mpg (-0.6%)	15.8 mpg (16%)	20.2 mpg (49%)
50-m following threshold	16.0 mpg (18%)	18.6 mpg (38%)	20.3 mpg (50%)
30-m following threshold	20.5 mpg (51%)	20.9 mpg (55%)	20.8 mpg (53%)

The simulation used the 2011 Toyota Camry as the test vehicle. The results show that even if the test vehicle utilizes the car-following-only mode on the I-81 study section, it can improve its fuel economy by 16 percent and 49 percent at 60 percent and 40 percent throttle levels, respectively. Using a 40 percent throttle level, the fuel economy of the test vehicle improves from 16 mpg to 20.3 mpg for the 50-m car-following threshold and from 20.5 mpg to 20.8 mpg for 30-m car-following threshold. Using a 40 percent throttle level improves the overall fuel efficiency, but it also produces longer vehicle spacings, as illustrated in **Figure 37**. When 40 percent throttle levels are employed in the proposed Eco-Driving system with a 50-m car-following threshold, the average spacing increases from 78 m to 99 m and the maximum spacing increases from 162 m to 277 m.

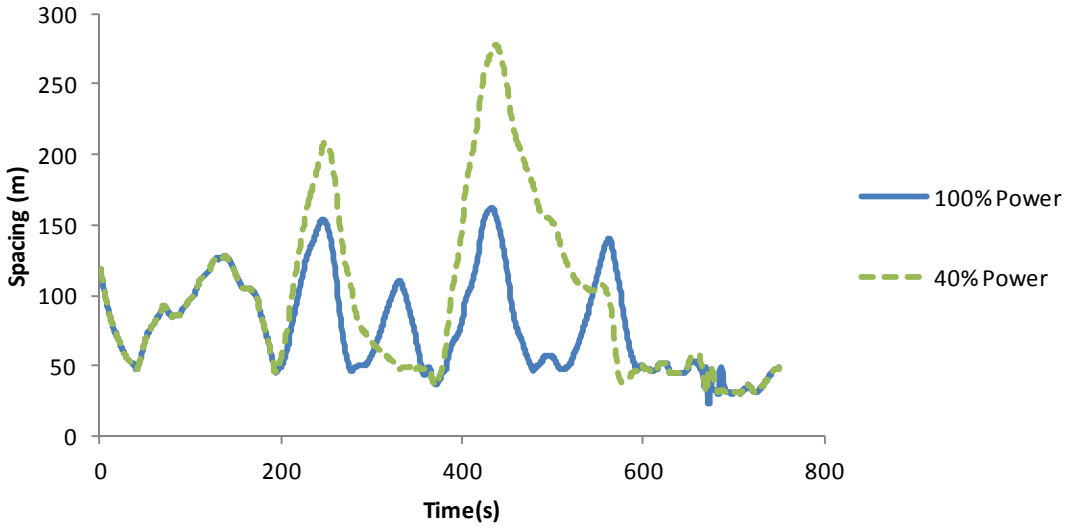

Figure 37. Spacing comparison of different power levels, Toyota Camry with 50-m threshold

6.4 Benefits of Following an ECC vehicle

The ECC vehicle generates an optimal vehicle control significant fuel saving benefits. This section investigates the benefits of following an ECC vehicle by putting the ECC vehicle in the lead position and a test vehicle in the following position using a car-following-only mode.

Figure 38 illustrates the speed profiles of the lead ECC vehicle and the test vehicle, which utilizes the proposed car-following algorithm. The simulation results demonstrate

that the ECC vehicle reduces its own fuel consumption by using the optimal vehicle control and that the test vehicle, a Toyota Camry, increases its fuel economy to 23.7 mpg just by following the lead ECC vehicle. It should be noted when the test vehicle is operated with the ECC-only mode, the test vehicle achieves a fuel economy of 24.6 mpg.

The simulation studies of the Chevy Tahoe and Malibu Hybrid reveal similar results. The Chevy Tahoe and Malibu Hybrid achieve fuel efficiencies of 14.3 mpg and 24.3 mpg, respectively, just by following a lead ECC vehicle on the study road section. The fuel efficiencies of the Chevy Tahoe and Malibu Hybrid under ECC operation are 14.3 mpg and 25.4 mpg. The results confirm that the fuel-saving benefit of following an ECC vehicle is as great as using the ECC system.

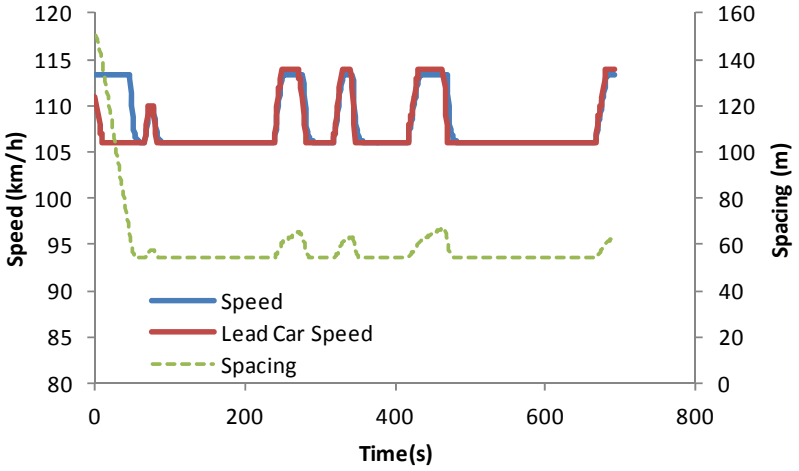

Figure 38. Following an ECC-equipped vehicle results

6.5 Lead Vehicle Lane Changing and Cut-in Scenario

The study investigates a lead vehicle lane change and cut-in scenario. The simulation uses the Toyota Camry as a test vehicle. As illustrated in Figure 28, a vehicle cut in at time 225 s and maintained a speed of 104 km/h for 5 min, then changed to another lane. A test vehicle using the proposed Eco-Driving system was simulated with a 30-m car-following threshold. When a vehicle cut in at time 225 s, the test vehicle reduced its speed to prevent a collision using the car-following mode and then a few seconds later the test vehicle was operated using the ECC mode. Also, at time 525 s when the lead vehicle left the lane, the test vehicle sped up to maintain a proper spacing and returned to the Eco-Driving system. The figure demonstrates that the proposed Eco-Driving system can effectively manage the lane changing and cut-in scenarios. The test vehicle achieved 18.4 mpg for the trip and maintained the average spacing of 50 m in this scenario.

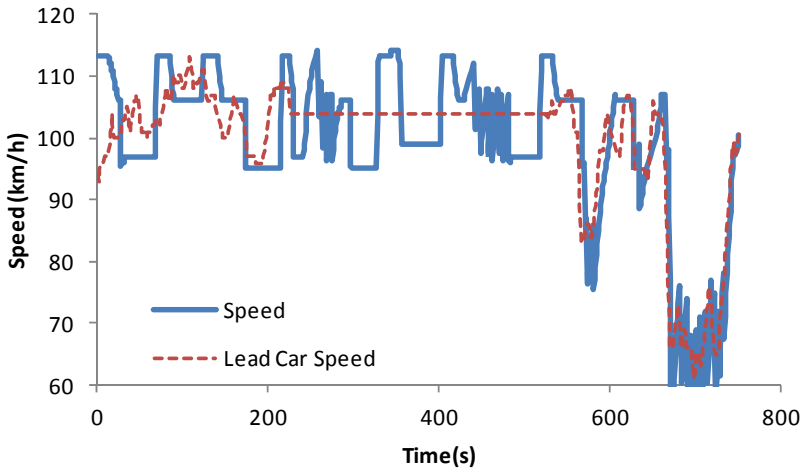

Figure 39. Lead car lane changing and cut-in scenario, Toyota Camry with 30-m threshold

7 Conclusions

The exploratory research investigated the potential of developing an Eco-Driving system that utilizes an ECC system within state-of-the-art car-following models. The system makes use of topographic information, the spacing data of lead vehicles, and a desired (or target) vehicle speed and distance headway as input variables. The proposed study focused on integrating predictive cruise control and optimal vehicle acceleration and deceleration controllers within car-following models. The exploratory study demonstrated that the proposed system can significantly improve fuel efficiency while maintaining reasonable vehicle spacing. One of the test vehicles, a 2011 Toyota Camry, saved 27 percent in fuel consumption with an average spacing of 48 m along the I-81 study section. The study also found that vehicle operations at lower power demands significantly enhance vehicle fuel economy (up to 49 percent), but not as significantly as the use of the ECC system (which improved fuel economy up to 82 percent). The study also demonstrated that non-ECC-equipped vehicles can significantly reduce their own fuel consumption just by following a lead ECC-equipped vehicle. Future research should quantify the potential benefits of using the proposed system at a network-wide level.

8 References

1. Ahn, K., H. Rakha, and K. Moran. *Eco-Cruise Control Systems: Feasibility and initial Testing*. in *Presented at 90th Annual Meeting of the Transportation Research Board*. 2011. Washington, D.C.
2. Park, S., H. Rakha, K. Ahn, and K. Moran. *Predictive Eco-Cruise Control: Algorithm and Potential Benefits*. in *IEEE forum on integrated and sustainable transportations systems(FISTS)*. 2011. Vienna, Austria.

3. Ecodrive.org. *What is Ecodriving*. 2011 Feb., 28 2011]; Available from: http://www.ecodrive.org/en/what_is_ecodriving-/.
4. McKinsey & Company, *Roads toward a low-carbon future: Reducing CO2 emissions from passenger vehicles in the global road transportation system*. 2009.
5. El-Shawarby, I., K. Ahn, and H. Rakha, *Comparative field evaluation of vehicle cruise speed and acceleration level impacts on hot stabilized emissions.* Transportation Research, Part D: Transport & Environment, 2005. 10(1): p. 13-30.
6. Nam, E.K., C.A. Gierczak, and J.W. Butler. *A Comparison of Real-World and Modeled Emissions Under Conditions of Variable Driver Aggressiveness*. in *Presented at 82th Annual Meeting of the Transportation Research Board*. 2003. Washington, D.C.
7. Tzirakis, E., K. Pitsas, F. Zannikos, and S. Stournas, *Vehicle Emissions and Driving Cycles: Comparison of The Athens Driving Cycle (ADC) with Ece-15 And European Driving Cycle (EDC).* Global NEST Journal, 2006. Vol 8(No 3): p. pp 282-290.
8. Nesamani, K.S. and K.P. Subramanian, *Impact of real-world driving characteristics on vehicular emissions.* JSME International Journal Series B-Fluids and Thermal Engineering, 2006. 49(1): p. 19-26.
9. Samuel, S., L. Austin, and D. Morrey, *Automotive test drive cycles for emission measurement and real-world emission levels - a review.* Proceedings of the Institution of Mechanical Engineers Part D-Journal of Automobile Engineering, 2002. 216(D7): p. 555-564.
10. Ericsson, E., *Variability in urban driving patterns.* Transportation Research Part D-Transport and Environment, 2000. 5(5): p. 337-354.
11. Ericsson, E., *Independent driving pattern factors and their influence on fuel-use and exhaust emission factors.* Transportation research. Part D, Transport and environment, 2001. Vol. 6D, no. 5 (Sept. 2001): p. p. 325-345.
12. De Vlieger, I., D. De Keukeleere, and J.G. Kretzschmar, *Environmental effects of driving behaviour and congestion related to passenger cars.* Atmospheric Environment, 2000. 34(27): p. 4649-4655.
13. National Research Council (U.S.), *Expanding metropolitan highways : implications for air quality and energy use*. 1995, Washington, D.C.: Transportation Research Board. viii, 387.
14. Ahn, K. and H. Rakha, *The effects of route choice decisions on vehicle energy consumption and emissions.* Transportation research. Part D, Transport and environment, 2008. 13(3): p. 17.
15. Kobayashi, I., Y. Tsubota, and H. Kawashima, *Eco-driving simulation : evaluation of eco-driving within a network using traffic simulation*, in *Urban transport XIII : urban transport and the environment in the 21st century. p. 741-750.* 2007, WIT press.
16. Jin, W., D. Yuan, and H. Yang. *A Study on Potential Environmental Benefits of Green Driving Strategies with NGSIM Data*. in *Presented at 90th Annual Meeting of the Transportation Research Board*. 2011. Washington, D.C.

17. Rafael-Morales, M. and J.C.D. Gortar, *Reduced consumption and environment pollution in Mexico by optimal technical driving of heavy motor vehicles.* Energy, 2002. 27(12): p. 1131-1137.

18. Zarkadoula, M., G. Zoidis, and E. Tritopoulou, *Training urban bus drivers to promote smart driving: A note on a Greek eco-driving pilot program.* Transportation Research Part D-Transport and Environment, 2007. 12(6): p. 449-451.

19. Larsson, H. and E. Ericsson, *The effects of an acceleration advisory tool in vehicles for reduced fuel consumption and emissions.* Transportation Research Part D-Transport and Environment, 2009. 14(2): p. 141-146.

20. Boriboonsomsin, K., A. Vu, and M. Barth, *Eco-Driving: Pilot Evaluation of Driving Behavior Changes among U.S. Drivers*. 2010, University of California Transportation Center.

21. Young, M.S., S.A. Birrell, and N.A. Stanton. *Design for Smart Driving: A Tale of Two Interfaces*. in *HCII 2009, LNAI 5639, pp. 477–485, 2009.* 2009.

22. Fairchild, R.G., J.F. Brake, N. Thorpe, S.A. Birrell, M.S. Young, T. Felstead, and M. Fowkes. *Using On-board Driver Feedback Systems to Encourage Safe, Ecological and Efficient Driving: The Foot-LITE Project*. in *The Society for the Study of Artificial Intelligence and Simulation of Behaviour Convention 6th - 9th April 2009*. 2009. Edinburgh, Scotland.

23. Barbé, J. and G. Boy. *Analysis and modelling methods for the design and evaluation of an eco-driving system*. in *European conference on Human Centred Design for Intelligent Transport Systems*. 2008. Lyon, France, April 3-4, 2008.

24. van der Voort, M., M.S. Dougherty, and M. van Maarseveen, *A prototype fuel-efficiency support tool.* Transportation Research Part C-Emerging Technologies, 2001. 9(4): p. 279-296.

25. Barth, M. and K. Boriboonsomsin, *Energy and emissions impacts of a freeway-based dynamic eco-driving system.* Transportation Research Part D-Transport and Environment, 2009. 14(6): p. 400-410.

26. Ando, R., Y. Nishihori, and D. Ochi, *Development of a System to Promote Eco-Driving and Safe-Driving* in *Lecture Notes in Computer Science, 2010, Volume 6294/2010, 207-218*. 2010.

27. Satou, K., R. Shitamatsu, M. Sugimoto, and E. Kamata, *DEVELOPMENT OF THE ON-BOARD ECO-DRIVING SUPPORT SYSTEM.* International Scientific Journal for Alternative Energy and Ecology 2010. No. 9 (89) 2010.

28. Lee, H., W. Lee, and Y.-K. Lim. *The effect of eco-driving system towards sustainable driving behavior*. in *CHI EA '10, Proceedings of the 28th of the international conference extended abstracts on Human factors in computing systems, 4255-4260*. 2010. Atlanta, GA.

29. Schwarzkopf, A.B. and R.B. Leipnik, *Control of Highway Vehicles for Minimum Fuel Consumption over Varying Terrain.* Transportation Research, 1977. 11(4): p. 279-286.

30. Hooker, J.N., *Optimal Driving For Single-Vehicle Fuel Economy.* Transportation research. Part A, Policy and practice, 1988. 22A(3): p. 183-201.

31. Hooker, J.N., A.B. Rose, and G.F. Roberts, *Optimal-Control of Automobiles for Fuel-Economy.* Transportation Science, 1983. 17(2): p. 146-167.

32. Lattemann, F., K. Neiss, S. Terwen, and T. Connolly, *The Predictive Cruise Control - A System to Reduce Fuel Consumption of Heavy Duty Trucks.* SAE International, 2004. 2004-01-2616.

33. Chang, D.J. and E.K. Morlok, *Vehicle Speed Profiles to Minimize Work and Fuel Consumption.* Journal of transportation engineering, 2005. 131(3): p. 10.

34. Hellstrom, E., *Explicit use of road topography for model predictive cruise control in heavy trucks*, in *Dept. of Electrical Engineering*. 2005, Linkopings unversitet.

35. Hellstrom, E., *Look-ahead control of heavy trucks utilizing road topography*, in *Electrical Engineering*. 2007, Linkopings University: Linkoping.

36. Hellstrom, E., A. Froberg, and L. Nielsen, *A Real-Time Fuel-Optimal Cruise Controller for Heavy Trucks Using Road Topography Information.* SAE International, 2006. 2006-01-0008.

37. Froberg, A., E. Hellstrom, and L. Nielsen, *Explicit Fuel Optimal Speed Profiles for Heavy Trucks on a Set of Topographic Road Profiles.* SAE International, 2006. 2006-01-1071.

38. Saboohi, Y. and H. Farzaneh, *Model for optimizing energy efficiency through controlling speed and gear ratio.* Energy Efficiency (2008) 1:65–76, 2008.

39. Saboohi, Y. and H. Farzaneh, *Model for developing an eco-driving strategy of a passenger vehicle based on the least fuel consumption.* Applied Energy, 2009. 86(10): p. 1925-1932.

40. Saerens, B., J. Vandersteen, T. Persoons, J. Swevers, M. Diehl, and E. Van den Buick, *Minimization of the fuel consumption of a gasoline engine using dynamic optimization.* Applied Energy, 2009. 86(9): p. 1582-1588.

41. Kamal, M.A.S., M. Mukai, J. Murata, and T. Kawabe. *Development of Ecological Driving System Using Model Predictive Control*. in *ICROS-SICE International Joint Conference 2009*. 2009. Fukuoka International Congress Center, Japan.

42. Kamal, M.A.S., M. Mukai, J. Murata, and T. Kawabe, *Ecological driver assistance system using model-based anticipation of vehicle-road-traffic information.* IET Intelligent Transport Systems, 2010. 4(4): p. 244-251.

43. Kamal, M.A.S., M. Mukai, J. Murata, and T. Kawabe. *On Board Eco-Driving System for Varying Road-Traffic Environments Using Model Predictive Control*. in *2010 IEEE International Conference on Control Applications*. 2010. Yokohama, Japan, September 8-10, 2010.

44. Marsden, G., M. McDonald, and M. Brackstone, *Towards an understanding of adaptive cruise control.* Transportation Research Part C-Emerging Technologies, 2001. 9(1): p. 33-51.

45. Ioannou, P.A. and M. Stefanovic, *Evaluation of ACC vehicles in mixed traffic: Lane change effects and sensitivity analysis.* Ieee Transactions on Intelligent Transportation Systems, 2005. 6(1): p. 79-89.

46. Zhang, J.L. and P.A. Ioannou, *Longitudinal control of heavy trucks in mixed traffic: Environmental and fuel economy considerations.* Ieee Transactions on Intelligent Transportation Systems, 2006. 7(1): p. 92-104.

47. Corona, D., M. Lazar, B. De Schutter, and M. Heemels. *A hybrid MPC approach to the design of a Smart adaptive cruise controller*. in *Computer Aided Control System Design, IEEE International Conference on Control Applications, 2006 pp231 - 236* 2006. Munich, Germany

48. Kohut, N., F. Borrelli, K. Hedrick, A. Lamprecht, J. Lee, C. Lee, and D. Rosario. *Utilization of intelligent transport systems information to increase fuel economy through engine control*. in *15th World Congress on Intelligent Transport Systems and ITS America's 2008 Annual Meeting*. 2008. New York NY.

49. Bageshwar, V.L., W.L. Garrard, and R. Rajamani, *Model predictive control of transitional maneuvers for adaptive cruise control vehicles.* Ieee Transactions on Vehicular Technology, 2004. 53(5): p. 1573-1585.

50. Li, S., K. Li, R. Rajamani, and J. Wang, *Model Predictive Multi-Objective Vehicular Adaptive Cruise Control.* IEEE TRANSACTIONS ON CONTROL SYSTEMS TECHNOLOGY, 2010. PP Issue:99 p. 1 - 11

51. Luo, L.H., H. Liu, P. Li, and H. Wang, *Model predictive control for adaptive cruise control with multi-objectives: comfort, fuel-economy, safety and car-following.* Journal of Zhejiang University-Science A, 2010. 11(3): p. 191-201.

52. Post, K., J.H. Kent, J. Tomlin, and N. Carruthers, *Fuel consumption and emission modeling by power demand and a comparison with other model.* Transportation Research, 1984. 18A: p. 191-213.

53. Akcelik, R., *Efficiency and drag in the power-based model of fuel consumption.* Transportation Research Part B-Methodological, 1989. 23B(5): p. 376-385.

54. Fisk, C.S., *Australian Road Research Board instantaneous model of fuel consumption.* Transportation Research Part B-Methodological, 1989. 23B(5): p. 373-376.

55. Barth, M., F. An, J. Norbeck, and M. Ross, *Modal emissions modeling: A physical approach.* Transportation Research Record, 1996(1520): p. 81-88.

56. Barth, M., F. An, T. Younglove, G. Scora, C. Levine, M. Ross, and T. Wenzel, *Comprehensive modal emission model (CMEM), version 2.0 user's guide*. 2000, Riverside, CA.

57. Frey, H.C., N.M. Rouphail, A. Unal, and J. Colyar. *Measurement of On-Road Tailpipe CO, NO, and Hydrocarbon Emissions Using a Portable Instrument*. in *Annual Meeting of the Air & Waste Management Association*. 2001. Orlando, Florida.

58. Huai, T., T.D. Durbin, T. Younglove, G. Scora, M. Barth, and J.M. Norbeck, *Vehicle specific power approach to estimating on-road NH3 emissions from light-duty vehicles.* Environmental Science & Technology, 2005. 39(24): p. 9595-9600.

59. Hellinga, B. and L. Fu, *Assessing Expected Accuracy of Probe Vehicle Travel Time Reports.* Journal of transportation engineering, 1999. 125(6): p. 7.

60. Hellinga, B., M.A. Khan, and L. Fu. *Analytical Emission Models for Signalised Arterials* in *The Canadian Society of Civil Engineers 3rd Transportation Specialty Conference*. 2000. London, Ontario, CA.

61. Hellinga, B.R., *Improving Freeway Speed Estimates from Single-Loop Detectors.* Journal of transportation engineering, 2002. 128(1): p. 10.

62. Ahn, K., H. Rakha, A. Trani, and M. Van Aerde, *Estimating vehicle fuel consumption and emissions based on instantaneous speed and acceleration levels.* Journal of Transportation Engineering-Asce, 2002. 128(2): p. 182-190.

63. Rakha, H., K. Ahn, K. Moran, B. Saerens, and E.V.d. Bulck, *Virginia Tech Comprehensive Power-Based Fuel Consumption Model: Model development and testing* Transportation research. Part D, Transport and environment, 2011. 16(7): p. 492-503

64. Rakha, H., K. Ahn, W. Faris, and K. Moran. *Simple Vehicle Driveline Model for use in Traffic Simulation Software*. in *89th Transportation Research Board Annual Meeting*. 2010. Washington D.C.

65. Ni, D. and D. Henclewood, *Simple Engine Models for VII-Enabled In-Vehicle Applications.* IEEE Transactions on Vehicular Technology, 2008. 57(5): p. 2695-2702.

66. Wong, J.Y., *Theory of Ground Vehicles*. Third ed. 2001: John Wiley & Sons, Inc.

67. Van Aerde, M. *Single regime speed-flow-density relationship for congested and uncongested highways*. in *74th TRB Annual Conference*. 1995. Washington DC.

68. Van Aerde, M. and H. Rakha. *Multivariate calibration of single regime speed-flow-density relationships*. in *Proceedings of the 6th 1995 Vehicle Navigation and Information Systems Conference*. 1995. Seattle, WA, USA: Vehicle Navigation and Information Systems Conference (VNIS) 1995. IEEE, Piscataway, NJ, USA,95CH35776..

69. Rakha, H. and M. Arafeh, *Calibrating Steady-State Traffic Stream and Car-following Models using Loop Detector Data.* Transportation Science, 2009. DOI: 10.1287/trsc.1090.0297.

70. Rakha, H., *Validation of Van Aerde's Simplified Steady-state Car-following and Traffic Stream Model.* Transportation Letters: The International Journal of Transportation Research, 2009. 1(3): p. 227-244.

71. Rakha, H. and I. Lucic, *Variable power vehicle dynamics model for estimating maximum truck acceleration levels.* Journal of Transportation Engineering, 2002. 128(5): p. 412-419.

72. Rakha, H., M. Snare, and F. Dion, *Vehicle dynamics model for estimating maximum light-duty vehicle acceleration levels.* Transportation Research Record, 2004. n 1883: p. 40-49.

73. Rakha, H., I. Lucic, S.H. Demarchi, J.R. Setti, and M. Van Aerde, *Vehicle dynamics model for predicting maximum truck acceleration levels.* Journal of Transportation Engineering, 2001. 127(5): p. 418-425.

U.S. Department of Transportation
ITS Joint Program Office-HOIT
1200 New Jersey Avenue, SE
Washington, DC 20590

Toll-Free “Help Line” 866-367-7487
www.its.dot.gov

FHWA-JPO-12-045